

# HOMOGENISATION OF A ROW OF DISLOCATION DIPOLES\*

STEPHEN JONATHAN CHAPMAN<sup>†</sup>, YANG XIANG<sup>‡</sup>, AND YICHAO ZHU<sup>‡</sup>

**Abstract.** Conventional discrete-to-continuum approaches have seen their limitation in describing the collective behaviour of the multi-polar configurations of dislocations, which are widely observed in crystalline materials. The reason is that dislocation dipoles, which play an important role in determining the mechanical properties of crystals, often get smeared out when traditional homogenisation methods are applied. To address such difficulties, the collective behaviour of a row of dislocation dipoles is studied by using matched asymptotic techniques. The discrete-to-continuum transition is facilitated by introducing two field variables respectively describing the dislocation pair density potential and the dislocation pair width. It is found by our analysis that the dislocation pair width evolves much faster than the pair density. Such hierarchy in evolution time enables us to describe the dislocation dynamics at the coarse-grained level by an evolution equation of the slowly varying variable (the pair density) coupled with an equilibrium equation of the fast varying variable (the pair width). The time-scale separation method adopted here also paves a way for properly incorporating dipole-like (zero net Burgers vector but non-vanishing) dislocation structures, known as the statistically stored dislocations (SSDs) into macroscopic models of crystal plasticity in three dimensions. Moreover, the natural transition between different equilibrium patterns found here may shed light on understanding the emergence of the persistent slip bands (PSBs) in fatigue metals induced by cyclic loads.

**Key words.** dislocations, homogenisation, asymptotic analysis, persistent slip bands

**AMS subject classifications.** 74A60, 74N15, 41A60

**1. Introduction.** It is well known that the plastic deformation of crystalline materials is carried by a large number of atomistic line defects, i.e. dislocations. Hence macroscopic models of crystal plasticity can be established by formulating the dynamics of considerably many dislocations. As an idealised (but also practically useful) case, the dynamics of straight and mutually-parallel dislocations have been intensively studied. These translationally invariant dislocations can be treated as “poles” on one of the planes perpendicular to all dislocation lines. These poles, like electrical charges, have signs depending on their line tangent with respect to the slip direction, known as the Burgers vector. Abundant experimental evidence suggests that a good understanding of the collective behaviour of many straight dislocations is important for controlling the mechanical properties of crystals. One example is found inside a fatigued single-crystalline copper specimen induced by cyclic loads [14]. Before the saturation point is reached, the inner configuration of the copper specimen takes a “channel-vein” structure as shown in Fig. 1(a). A vein consists of many almost straight and closely spaced edge dislocations and the veins are separated by channels where the dislocation density is relatively low. Beyond the saturation point, a characteristic ladder-shape structure known as the persistent slip bands (PSBs) is found forming as shown in Fig. 1(b). The walls of the ladders also consist of straight edge dislocations. The mechanism governing the transition between the channel-vein to PSB structures is still unclear and a study of the collective behaviour of edge dipoles can be of great help to its understanding.

---

\*This work was partly supported by EPSRC through grant EP/D048400/1, and by the Hong Kong Research Grants Council through General Research Fund 606313

<sup>†</sup>Mathematical Institute, University of Oxford, Andrew Wiles Building, Radcliffe Observatory Quarter, Woodstock Road, Oxford, OX2 6GG, UK. (chapman@maths.ox.ac.uk).

<sup>‡</sup>Department of Mathematics, the Hong Kong University of Science and Technology, Clear Water Bay, Kowloon, Hong Kong, China. (maxiang@ust.hk and mayczhu@ust.hk).

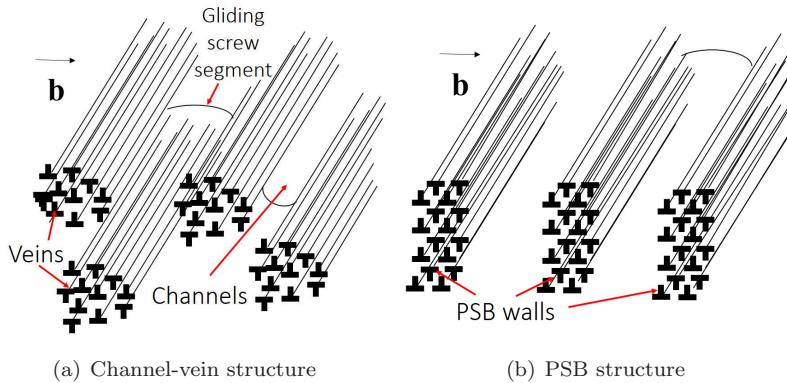


FIG. 1. Dislocation patterns in the early stage of metal fatigue induced by cyclic loads.

One way to reveal the role of these straight dislocations played during the formation of PSBs, is by using the two-dimensional (2D) discrete dislocation dynamical (DDD) models, where all dislocations are tracked individually (e.g. [3]). Nevertheless, it appears still difficult to get a clear picture over the mechanism that governs the dislocation pattern formation in crystals from the DDD simulation methods. Hence there are still necessities of investigating the dynamics of dislocations at a continuous level, where materials substructures are described by a dislocation density distribution field. In principle, a dislocation-density-based continuum model should be obtained by means of a rigorous summary of its underlying 2D DDD model. However, it turns out that all existing discrete-to-continuum approaches have seen their limitation in the upscaling of the multi-polar configurations of straight dislocations. The reason is as follows. At room temperature, dislocations (of edge types) are in general constrained in their own slip planes. As a result, an edge dislocation defined in a positive sense tends to form a pair of dipole, which is neutral and tiny in size, with a nearby dislocation defined in a negative sense rather than to annihilate with each other, if they do not belong to a same slip plane. Such dipolar locks effectively increase the strength of crystals. When traditional homogenisation methods are applied, however, the role of dipoles which is crucial in determining the material mechanical properties, gets completely smeared out. Owing to this, traditional homogenisation techniques are only applicable to investigate the collective behaviour of many monopoles (dislocations of the same sign) (e.g. [7, 15, 16]), and the collective behaviour of an arbitrary multi-dislocation-pole configuration is only considered in a statistical or phenomenological manner [5, 8, 9]. There have also been works studying the collective behaviour of dipoles in [10], which treats each dipole pair as one object so that the traditional homogenisation method can be applied. As shown by our analysis, this only works in the case where the slip plane spacing is much smaller compared to the distance between the centers of two neighbouring dipoles.

The challenge posed by dipoles in 2D space also addresses the main difficulties in the entrenchment of a dislocation-density-based continuum model in three-dimensional space, which has drawn attentions of many researchers for the past two decades (e.g. [2, 4, 6, 11, 13]). At the continuum level, the dislocation density distribution fields are introduced through the homogenisation of dislocation ensembles within a small volume. Consequentially, the dislocation density fields defined by this way only take into account the density distributions of the geometrically necessary dislocations

(GNDs). What are smeared out by the homogenisation process are the mechanisms due to local dislocation-dislocation interactions such as dislocation line tangent effect and the statistically stored dislocations (SSDs), whose physical dimensions are smaller than the volume over which the average is taken. In three-dimensional space, the SSD structures that account for the macroscopic mechanical properties of crystals include small dislocation loops either due to source operation or thermal fluctuation, mutually locked dislocation segments like dislocation dipoles, etc. Therefore, a pivotal question to be answered for the entrenchment of a solid dislocation-density-based model is, “by what means the effects due to such short-range dislocation-dislocation interactions and SSDs should be maintained at a coarse-grained scale?” Part of the question has been answered through the establishment of a continuum model of plasticity, where a set of dislocation density potential functions (DDPFs) are employed to represent the dislocation substructures on a single slip plane [17, 18, 21] and in three-dimensional space [22]. The micro-scale mechanisms that are well incorporated into the continuum model underlain by the DDPFs are the dislocation line tangent effect [17], the grain boundary structures [19] and the operation of dislocation sources of the Frank-Read type [21]. The hints of how to effectively incorporate SSDs at the continuum level can be found from the analysis presented in this paper.

Motivated by these purposes, the collective behaviour of a row of dislocation dipoles is rigorously studied here. The discrete-to-continuum transition is facilitated by the introduction of two field variables respectively describing the dislocation pair density potential and the dislocation pair width. By using asymptotic analysis, the dynamical relation of the row of dipoles at the continuum level, is expected to be described by the evolution equations of the two introduced field variables. Actually it is shown that the time scales associated with the two field variables are different. The dislocation pair width, which moves in response to the resolved shear stress at the leading order, varies at a time scale much faster than that associated with the dislocation pair density moving in response to the “stress gradient” (coming from the resolved shear stress at the next order). Hence if viewed at the slower scale, fast-varying mechanisms take place so quickly that only their steady (or equilibrium) states need to be taken into account. As a result, the collective behaviour of a row of dislocation dipoles at the continuum level can be described by an evolution equation of the slowly varying dislocation pair density and an equilibrium equation of the fast varying dislocation pair width. Such discrete-to-continuum approaches by asymptotically separating active processes according to their associated time scales may pave a way for the incorporation of SSDs at the continuum level. Moreover, a transition between two discrepant dipolar patterns due to instability, which was originally discovered in periodically distributed dipoles [20], is also seen here and the transition may be indicative to the reason of PSB formation.

The paper is arranged as follows. The governing equations for the DDD model, which is the reference model in this paper, are firstly written down in §2. After the introduction of the variables needed for the discrete-to-continuum transition in §3, we derive for the asymptotic expressions of the resolved stress field in §4. Then the governing equations for equilibrium states and the dynamical relations at the continuum level are presented in §5. In §6, the equilibrium states at the continuum level are further analysed and a natural transition between different equilibrium patterns are found. In §7, the accuracy and efficiency of the derived continuum model are studied. The article concludes further discussion on the derived continuum model made in §8.

**2. Dynamics at the level of discrete dislocations.** Here we consider the case of a single slip system associated with the Burgers vector denoted by  $\mathbf{b}$ , and all dislocations here are straight, mutually parallel and of edge type. The problem is thus reduced to one of the planes that are orthogonal to all dislocation tangents. Here the plane of interest is set to be the  $x$ - $y$  plane as shown in Fig. 2. Each dislocation is thus

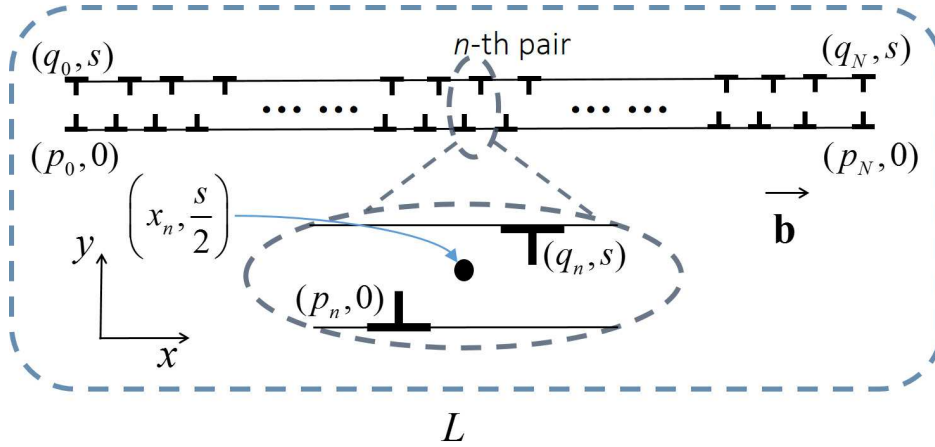


FIG. 2. The  $x$ - $y$  plane is one of the planes perpendicular to all dislocation lines. The numbers of positive and negative dislocations are identically  $N+1$ . All positively oriented dislocations are located on one slip plane, which degenerates to the  $x$ -axis here, and all negatively oriented dislocations are put on another slip plane at a distance of  $s$  from the  $x$ -axis (given by  $y = s$ ). The  $n$ -th dislocation pair consists of the  $n$ -th positive and negative dislocations, whose locations are set to be at  $(p_n, 0)$  and  $(q_n, s)$ , respectively. The  $x$  coordinate for the center of the  $n$ -th pair is denoted by  $x_n$  given by Eq. (2.1). Here  $L$  is the distance between the leftmost and rightmost pair centers and  $\mathbf{b}$  is the Burgers vector.

treated as a signed pole in  $x$ - $y$  plane. Here a dislocation pointing into the paper plane is set to be a positively oriented dislocation (termed as a “positive dislocation” here) and denoted by “ $\perp$ ”, while a dislocation pointing outward the paper plane is set to be a negatively oriented dislocation (termed as a “negative dislocation”) and denoted by “ $\top$ ”.

The configuration considered here is shown in Fig. 2. There are  $N + 1$  positive dislocations lying on the slip plane given by the  $x$ -axis, while  $N + 1$  negative dislocations are put on another slip plane at a distance of  $s$  from the  $x$ -axis. The  $n$ -th dislocation pair is set to consist of the  $n$ -th positive and negative dislocations, which are located at  $(p_n, 0)$  and  $(q_n, s)$ , respectively. The  $x$ -coordinate of the center of the  $n$ -th pair denoted by  $x_n$  is thus expressed by

$$(2.1) \quad x_n = \frac{p_n + q_n}{2}.$$

Concerning the motion of dislocations, we employ an empirical dislocation mobility law, which only allow dislocations (of edge types) to glide within their slip plane at a speed in proportion to their on-site resolved shear stresses. Under this rule, the motion of the  $n$ -th positive dislocation is given by

$$(2.2) \quad v_n^+ = \frac{dp_n}{dt} = m_g b (\tau_{\text{int}}(p_n, 0) + \tau_{\text{ext}}(p_n, 0)),$$

where  $v_n^+$  denotes the speed of the  $n$ -th positive dislocation along  $x$ -direction;  $\tau_{\text{int}}(x, y)$  is the internal resolved shear stress field at  $(x, y)$  resulting from the dislocation-dislocation interactions;  $\tau_{\text{ext}}(x, y)$  denotes the externally applied resolved shear stress at  $(x, y)$ ;  $m_g$  is the dislocation glide coefficient;  $b = |\mathbf{b}|$ . Analogically, the gliding speed of the  $n$ -th negative dislocation is governed by

$$(2.3) \quad v_n^- = \frac{dq_n}{dt} = -m_g b (\tau_{\text{int}}(q_n, s) + \tau_{\text{ext}}(q_n, s)),$$

where it is worth noting that the negative sign in the right hand side of Eq. (2.3) suggests that, a positive and a negative dislocation move along opposite directions under a same resolved shear stress field.

Throughout this paper, we use the Greek letter  $\tau$  associated with a super- or subscript to denote resolved shear stress components due to various sources. The internal resolved shear stress field  $\tau_{\text{int}}(p_n, 0)$  is calculated by the superposition of the resolved shear stresses due to all individual dislocations [12]

$$(2.4) \quad \tau_{\text{int}}(p_n, 0) = \frac{\mu b}{2\pi(1-\nu)} \sum_{\substack{j=0 \\ j \neq n}}^N \frac{1}{p_n - p_j} - \frac{\mu b}{2\pi(1-\nu)} \sum_{j=0}^N \frac{(p_n - q_j)((p_n - q_j)^2 - s^2)}{((p_n - q_j)^2 + s^2)^2}.$$

Similarly, the internal resolved shear stress at  $(q_n, s)$  is calculated by

$$(2.5) \quad \tau_{\text{int}}(q_n, s) = \frac{\mu b}{2\pi(1-\nu)} \sum_{j=0}^N \frac{(q_n - p_j)((q_n - p_j)^2 - s^2)}{((q_n - p_j)^2 + s^2)^2} - \frac{\mu b}{2\pi(1-\nu)} \sum_{\substack{j=0 \\ j \neq n}}^N \frac{1}{q_n - q_j}.$$

Hence the dynamics at the level of discrete dislocations is formulated by Eqs. (2.2) - (2.5), which form a closed system of ordinary differential equations with  $2(N+1)$  unknowns  $\{p_n\}_{n=0}^N$  and  $\{q_n\}_{n=0}^N$ .

**3. Set-up for discrete-to-continuum transition.** Usually the number of dislocations in crystals is very large. Hence it is sensible to consider the collective behaviour of the system governed by Eqs. (2.2) - (2.5). Mathematically, this can be achieved by examining the asymptotic behaviour of the above equation system with  $N \rightarrow \infty$ . The expected outcomes are the evolution equations of some continuously defined variables that characterise the dislocation substructures. In this section, we will introduce these field variables needed for the discrete-to-continuum transition after we non-dimensionalise all variables.

**3.1. Non-dimensionalisation.** Recalling that  $L$  is the length of the domain of interest as shown in Fig. 2, we non-dimensionalise all spatial variables by  $L$ , all stress components by  $\mu N b / (2\pi(1-\nu)L)$  and time  $t$  by  $2\pi(1-\nu)L^2 / (\mu m_g N b^2)$ . Throughout the paper, a hat is put on a variable to denote its non-dimensionalised counterpart. Hence the non-dimensionalised version of the above equation system becomes

$$(3.1) \quad \frac{d\hat{p}_n}{d\hat{t}} = \hat{\tau}_{\text{int}}(\hat{p}_n, 0) + \hat{\tau}_{\text{ext}}(\hat{p}_n, 0),$$

$$(3.2) \quad \frac{d\hat{q}_n}{d\hat{t}} = -\hat{\tau}_{\text{int}}(\hat{q}_n, \hat{s}) - \hat{\tau}_{\text{ext}}(\hat{q}_n, \hat{s}),$$

$$(3.3) \quad \hat{\tau}_{\text{int}}(\hat{p}_n, 0) = \frac{1}{N} \sum_{\substack{j=0 \\ j \neq n}}^N \frac{1}{\hat{p}_n - \hat{p}_j} - \frac{1}{N} \sum_{j=0}^N \frac{(\hat{p}_n - \hat{q}_j)((\hat{p}_n - \hat{q}_j)^2 - \hat{s}^2)}{((\hat{p}_n - \hat{q}_j)^2 + \hat{s}^2)^2}$$

and

$$(3.4) \quad \hat{\tau}_{\text{int}}(\hat{q}_n, \hat{s}) = \frac{1}{N} \sum_{j=0}^N \frac{(\hat{q}_n - \hat{p}_j)((\hat{q}_n - \hat{p}_j)^2 - \hat{s}^2)}{((\hat{q}_n - \hat{p}_j)^2 + \hat{s}^2)^2} - \frac{1}{N} \sum_{\substack{j=0 \\ j \neq n}}^N \frac{1}{\hat{q}_n - \hat{q}_j}.$$

Here we only consider the case when  $\hat{s}$ , the non-dimensionalised spacing between the two slip planes, is as small as  $\mathcal{O}(1/N)$ , where  $\mathcal{O}$  means “the order of”. This implies that  $\hat{s}$  can be rescaled by

$$(3.5) \quad S = \frac{\hat{s}}{N},$$

where  $S \sim \mathcal{O}(1)$ . When  $\hat{s} \sim \mathcal{O}(1)$ , the slip planes are so well separated that the configuration can be treated as two rows of isolated monopoles, which can be studied by applying conventional homogenisation approaches.

**3.2. Variables needed for the discrete-to-continuum transition.** Given a large  $N$ , the length scale associated with the discrete dislocation dynamical model given by Eqs. (3.1) to (3.4) is characterised by the neighbouring spacings of the discrete dislocations, i.e.  $\mathcal{O}(1/N)$ , so that individual dislocations can be observed. Now we want to describe the same dynamical relation by a model associated with the length scale at  $\mathcal{O}(1)$ , where no isolated dislocations, but the continuous dislocation density distribution is considered. For consistency, the model built at the continuum level (termed as the “continuum model” in this paper), should be entrenched by means of a rigorous discrete-to-continuum transition, that is, reformulating Eqs. (3.1) to (3.4) by using matched asymptotic techniques.

To facilitate such transition, we first introduce a continuous function of (non-dimensionalised) time and space denoted by  $\zeta(\hat{t}, \hat{x})$ , such that

$$(3.6) \quad \frac{\zeta(\hat{t}, \hat{x}_n)}{N} = \hat{q}_n - \hat{p}_n,$$

where according to Eq. (2.1),  $\hat{x}_n$  is the  $\hat{x}$  coordinate for the center of the  $n$ -th dislocation pair given by

$$(3.7) \quad \hat{x}_n = \frac{\hat{p}_n + \hat{q}_n}{2}.$$

Here  $\zeta(\hat{t}, \hat{x})$  is a field variable defined for  $\hat{x} \in [0, 1]$ , and its value at  $\hat{x}_n$  measures the width of  $n$ -th dislocation pair scaled by  $N$  according to Eq. (3.8). Since the spacings of neighbouring dislocations are at  $\mathcal{O}(1/N)$ ,  $\zeta(\hat{t}, \hat{x}) \sim \mathcal{O}(1)$ . Viewed at the continuum level,  $\zeta$  is employed to characterise the local patterns of dislocation dipoles.

Throughout the paper, a superscript  $n$  or  $j$  affiliated with a field variable such as  $\zeta$  indicates that the field is evaluated at  $\hat{x} = \hat{x}_n$  or at  $\hat{x} = \hat{x}_j$ , respectively, for example,

$$(3.8) \quad \zeta_n = \zeta(\hat{t}, \hat{x}_n).$$

Without loss of generality, we consider the case where  $\zeta \in [0, 1/2]$ .

Hence  $\hat{p}_n$  and  $\hat{q}_n$  can both be expressed in terms of  $\hat{x}_n$  and  $\zeta_n$  by

$$(3.9) \quad \hat{p}_n = \hat{x}_n - \frac{\zeta_n}{2N}$$

and

$$(3.10) \quad \hat{q}_n = \hat{x}_n + \frac{\zeta_n}{2N},$$

respectively.

We then introduce another field variable, the dislocation pair density potential  $\phi(\hat{t}, \hat{x})$ , such that

$$(3.11) \quad \phi(\hat{t}, \hat{x}_n) = \frac{n}{N} := \phi_n,$$

where  $:=$  denotes “defined to be”. Actually  $\phi$  here is introduced in analogy with the dislocation density potential functions defined by [17] or [22]. It can be shown by following the same argument presented in [17] that, the density distribution of the dislocation pairs denoted by  $\rho$  can be calculated by

$$(3.12) \quad \rho = \frac{\partial \phi}{\partial \hat{x}}.$$

Throughout this paper, the inputs  $(\hat{t}, \hat{x})$  for  $\phi$  and  $\zeta$  are omitted if no ambiguities are caused. Moreover, a dash is added to a variable to denote its derivative with respect to  $\hat{x}$ . For example,

$$(3.13) \quad \phi' = \frac{\partial \phi}{\partial \hat{x}}, \quad \phi'' = \frac{\partial^2 \phi}{\partial \hat{x}^2}, \quad \dots$$

By doing that, we have  $\rho = \phi'$ .

Therefore, at the continuum level, the dislocation substructures are expected to be described by the two field variables  $\phi$  and  $\zeta$  and the goal now is to look for their governing equations by means of upscaling Eqs. (3.1) - (3.4).

**4. Asymptotic behaviour of the resolved shear stress field.** In this paper the discrete-to-continuum transition usually takes the following procedures. Given a quantity defined in a discrete sense, we first asymptotically express the quantity values at  $(\hat{p}_n, 0)$  and  $(\hat{q}_n, \hat{s})$  by functions of  $\hat{x}_n$ , for any integer  $n \in [0, N]$ . Thus the equations set up at the discrete level can be transformed into asymptotic equations of  $\phi$  and  $\zeta$ , which only hold at every  $\hat{x}_n$ . Then by using the fact that  $\hat{x}_n$  is densely distributed throughout the whole domain, we replace  $\hat{x}_n$  by  $\hat{x}$  to turn the obtained equations to their corresponding integral-differential equations of  $\phi$  and  $\zeta$ , which hold for all  $\hat{x}$ .

Following this strategy, we start by considering the asymptotic behaviour of the internal resolved shear stress  $\hat{\tau}_{\text{int}}(\hat{p}_n, 0)$  and  $\hat{\tau}_{\text{int}}(\hat{q}_n, \hat{s})$ , given by Eq. (3.3) and (3.4), respectively as  $N \rightarrow \infty$ . First, an interval  $\Omega_{\text{in}}^n$  is introduced associated with the  $n$ -th dislocation pair, such that the  $\hat{x}$ -coordinates of the centers of its  $2K$  neighbouring pairs fall inside  $\Omega_{\text{in}}^n$  as shown in Fig. 3. The number  $K$  here satisfies

$$(4.1) \quad 1 \ll K \ll N.$$

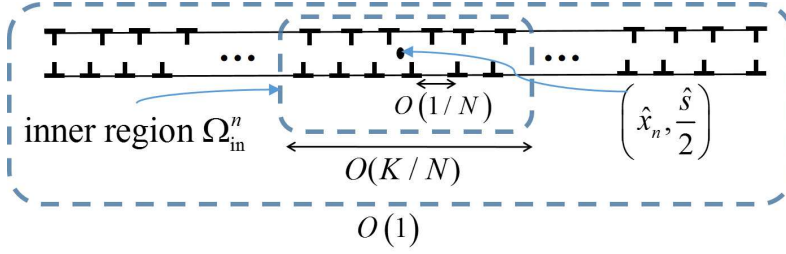


FIG. 3. Given the  $n$ -th dislocation pair, the  $\hat{x}$ -coordinates of the centers of its  $2K$  neighbouring pairs fall inside an interval, defined to be the inner region  $\Omega_{\text{in}}^n$ , whose size is at  $\mathcal{O}(K/N)$ . Mathematically, this interval is given by Eq. (4.2). The outer region is defined to be the interval, into which the  $\hat{x}$ -coordinates of the centers of all other dislocation pairs fall. Mathematically, it is given by Eq. (4.3).

Throughout this paper,  $\Omega_{\text{in}}^n$  defined in this way is termed as the “inner region”. Mathematically,  $\Omega_{\text{in}}^n$  is represented by

$$(4.2) \quad \Omega_{\text{in}}^n = \left\{ \hat{x} \left| \left| \phi(\hat{t}, \hat{x}) - \frac{n}{N} \right| \leq \frac{K}{N} \right. \right\}.$$

It can be seen that the length of  $\Omega_{\text{in}}^n$  is at  $\mathcal{O}(K/N)$ . Analogously we define an “outer region” by

$$(4.3) \quad \Omega_{\text{out}}^n = \left\{ \hat{x} \left| \left| \phi(\hat{t}, \hat{x}) - \frac{n}{N} \right| > \frac{K}{N} \right. \right\},$$

which contains the  $\hat{x}$ -coordinate of the centers of all other dislocation pairs. Then we can estimate  $\hat{\tau}_{\text{int}}(\hat{p}_n, 0)$  in Eq. (3.3) by decomposing it into two parts

$$(4.4) \quad \hat{\tau}_{\text{int}}(\hat{p}_n, 0) = \hat{\tau}_{\text{int}}^{\text{in}}(\hat{p}_n, 0) + \hat{\tau}_{\text{int}}^{\text{out}}(\hat{p}_n, 0),$$

where  $\hat{\tau}_{\text{int}}^{\text{in}}(\hat{p}_n, 0)$  denotes the resolved shear stress due to all dislocations associated with the inner region  $\Omega_{\text{in}}^n$

$$(4.5) \quad \hat{\tau}_{\text{int}}^{\text{in}}(\hat{p}_n, 0) = \sum_{\substack{j=n-K \\ j \neq n}}^{n+K} \frac{1}{\hat{p}_n - \hat{p}_j} - \sum_{j=n-K}^{n+K} \frac{(\hat{p}_n - \hat{q}_j)((\hat{p}_n - \hat{q}_j)^2 - \hat{s}^2)}{((\hat{p}_n - \hat{q}_j)^2 + \hat{s}^2)^2}$$

and  $\hat{\tau}_{\text{int}}^{\text{out}}(\hat{p}_n, 0)$  denotes the resolved shear stress due to all dislocations associated with  $\Omega_{\text{out}}^n$

$$(4.6) \quad \hat{\tau}_{\text{int}}^{\text{out}}(\hat{p}_n, 0) = \sum_{\substack{0 \leq j < n-K \\ n+K < j \leq N}} \left( \frac{1}{\hat{p}_n - \hat{p}_j} - \frac{(\hat{p}_n - \hat{q}_j)((\hat{p}_n - \hat{q}_j)^2 - \hat{s}^2)}{((\hat{p}_n - \hat{q}_j)^2 + \hat{s}^2)^2} \right).$$

It is worth noting that the decomposition suggested by Eq. (4.4) only holds for dislocation pairs that are not too close to the boundaries, i.e.  $K < n < N - K$ . We will go back to this issue in §6.1.2.

In a similar manner,  $\hat{\tau}(\hat{q}_n, \hat{s})$  in Eq. (3.4) can be decomposed by

$$(4.7) \quad \hat{\tau}_{\text{int}}(\hat{q}_n, \hat{s}) = \hat{\tau}_{\text{int}}^{\text{in}}(\hat{q}_n, \hat{s}) + \hat{\tau}_{\text{int}}^{\text{out}}(\hat{q}_n, \hat{s}),$$

where

$$(4.8) \quad \hat{\tau}_{\text{int}}^{\text{in}}(\hat{q}_n, \hat{s}) = \sum_{j=n-K}^{n+K} \frac{(\hat{q}_n - \hat{p}_j)((\hat{q}_n - \hat{p}_j)^2 - \hat{s}^2)}{((\hat{q}_n - \hat{p}_j)^2 + \hat{s}^2)^2} - \sum_{\substack{j=n-K \\ j \neq n}}^{n+K} \frac{1}{\hat{q}_n - \hat{q}_j}$$

and

$$(4.9) \quad \hat{\tau}_{\text{int}}^{\text{out}}(\hat{q}_n, \hat{s}) = \sum_{\substack{0 \leq j < n-K \\ n+K < j \leq N}} \left( \frac{(\hat{q}_n - \hat{p}_j)((\hat{q}_n - \hat{p}_j)^2 - \hat{s}^2)}{((\hat{q}_n - \hat{p}_j)^2 + \hat{s}^2)^2} - \frac{1}{\hat{q}_n - \hat{q}_j} \right).$$

**4.1. Inner region approximation.** In order to get the asymptotic expressions for  $\hat{\tau}_{\text{int}}^{\text{in}}(\hat{p}_n, 0)$ , we first look for the expansion of each term in the summation appearing in Eq. (4.5). Given a dislocation associated with the inner region, the distance from its  $\hat{x}$ -coordinate, for example,  $\hat{p}_j$  or  $\hat{q}_j$ , to  $\hat{x}_n$ , the  $\hat{x}$ -coordinate of the center of  $n$ -th dislocation pair is small compared to the length of the computational domain, which equals to 1 after non-dimensionalisation. Hence we can use Taylor expansion to asymptotically express  $\hat{p}_j$  and  $\hat{q}_j$  near  $\hat{x}_n$ . This is found taking two steps: first relating  $\hat{p}_j$  and  $\hat{q}_j$  to  $\hat{x}_j$  and then relating  $\hat{x}_j$  to  $\hat{x}_n$ . The first step has been achieved by Eqs. (3.9) and (3.10). For the second step, we re-write Eq. (3.11) by

$$(4.10) \quad \phi(\hat{t}, \hat{x}_j) = \frac{j}{N} = \frac{n}{N} + \frac{j-n}{N} = \phi(\hat{t}, \hat{x}_n) + \frac{j-n}{N}.$$

If setting  $\phi^{-1}(j/N) = \hat{x}_j$ , which is effectively the inverse function of  $\phi(\hat{t}, \hat{x})$  in  $\hat{x}$ , we can then take  $\phi^{-1}$  on both sides of Eq. (4.10) to obtain

$$(4.11) \quad \hat{x}_j = \phi^{-1} \left( \phi(\hat{t}, \hat{x}_n) + \frac{j-n}{N} \right).$$

Since  $|\frac{j-n}{N}| \leq \frac{K}{N} \ll 1$  hold for all  $\hat{x}_j \in \Omega_{\text{in}}^n$ , one can expand Eq. (4.11) in terms of  $\frac{j-n}{N}$  to obtain

$$(4.12) \quad \hat{x}_j \sim \hat{x}_n + \frac{j-n}{N} \cdot \frac{1}{\phi'_n} - \frac{(j-n)^2}{N^2} \cdot \frac{\phi''_n}{2(\phi'_n)^3} + \frac{(j-n)^3}{N^3} \cdot \frac{(3(\phi''_n)^2 - \phi'_n \phi'''_n)}{6(\phi'_n)^5} + \mathcal{O} \left( \frac{K^4}{N^4} \right).$$

It is worth to be reminded that an index  $n$  put to  $\phi$  or  $\zeta$  suggests the evaluation is made at  $\hat{x}_n$ . With Eq. (4.12), we obtain the expansion of  $\zeta_j$  near  $\zeta_n$  in terms of  $\frac{j-n}{N}$  by

$$(4.13) \quad \zeta_j = \zeta(\hat{t}, \hat{x}_j) \sim \zeta_n + \frac{1}{N} \cdot \frac{(j-n)\zeta'_n}{\phi'_n} + \frac{1}{N^2} \cdot \frac{(j-n)^2(\zeta''_n \phi'_n - \phi''_n \zeta'_n)}{2(\phi'_n)^3} + \mathcal{O} \left( \frac{K^3}{N^3} \right).$$

Hence combining Eqs. (3.9), (4.12) and (4.13), we can asymptotically express  $\hat{p}_j$  near  $\hat{x}_n$  by

$$(4.14) \quad \begin{aligned} \hat{p}_j \sim \hat{x}_n + \frac{1}{N} \cdot \left( \frac{j-n}{\phi'_n} - \frac{\zeta_n}{2} \right) - \frac{1}{2N^2} \cdot \left( \frac{(j-n)\zeta'_n}{\phi'_n} + \frac{(j-n)^2 \phi''_n}{(\phi'_n)^3} \right) \\ + \frac{(j-n)^2}{N^3} \cdot \left( \frac{\zeta'_n \phi''_n}{4(\phi'_n)^3} + \frac{(j-n)\phi''_n}{2(\phi'_n)^5} - \frac{\zeta''_n}{4(\phi'_n)^2} - \frac{(j-n)\phi'''_n}{6(\phi'_n)^4} \right) + \mathcal{O} \left( \frac{K^4}{N^4} \right). \end{aligned}$$

Similarly we have

$$(4.15) \quad \hat{q}_j \sim \hat{x}_n + \frac{1}{N} \cdot \left( \frac{j-n}{\phi'_n} + \frac{\zeta_n}{2} \right) + \frac{1}{2N^2} \cdot \left( \frac{(j-n)\zeta'_n}{\phi'_n} - \frac{(j-n)^2\phi''_n}{(\phi'_n)^3} \right) \\ - \frac{(j-n)^2}{N^3} \cdot \left( \frac{\zeta'_n\phi''_n}{4(\phi'_n)^3} - \frac{(j-n)\phi''_n}{2(\phi'_n)^5} - \frac{\zeta''_n}{4(\phi'_n)^2} + \frac{(j-n)\phi'''_n}{6(\phi'_n)^4} \right) + \mathcal{O}\left(\frac{K^4}{N^4}\right).$$

Then incorporating Eqs. (4.14) and (4.15) into (4.5), we obtain the expansion of  $\hat{\tau}_{\text{int}}^{\text{in}}(\hat{p}_n, 0)$  as

$$(4.16) \quad \hat{\tau}_{\text{int}}^{\text{in}}(\hat{p}_n, 0) \sim (\pi\phi'_n) \cdot G_0(2\pi\zeta_n\phi'_n, 2\pi S\phi'_n) + \frac{2\zeta_n\phi'_n}{K} - \frac{\zeta_n\phi'_n}{K^2} \\ - \frac{\phi''_n}{N\phi'_n} \cdot G_{11}(2\pi\zeta_n\phi'_n, 2\pi S\phi'_n) - \frac{(\zeta_n\phi'_n)'}{N} \cdot G_{12}(2\pi\zeta_n\phi'_n, 2\pi S\phi'_n) \\ - \frac{\phi'_n\zeta'_n}{N} \cdot G_{13}(2\pi\zeta_n\phi'_n, 2\pi S\phi'_n) + o\left(\frac{1}{N}\right),$$

where

$$(4.17) \quad G_0(\alpha, \beta) = \frac{\sin \alpha}{\cosh \beta - \cos \alpha} - \frac{\beta \sin \alpha \sinh \beta}{(\cos \alpha - \cosh \beta)^2},$$

(4.18)

$$G_{11}(\alpha, \beta) = -\frac{1}{2} - \frac{\alpha \sin \alpha + 2\beta \sinh \beta}{2(\cos \alpha - \cosh \beta)} + \frac{5\beta^2(1 - \cos \alpha \cosh \beta)}{4(\cos \alpha - \cosh \beta)^2} - \frac{3\alpha\beta \sin \alpha \sinh \beta}{2(\cos \alpha - \cosh \beta)^2} \\ + \frac{\beta^3 \sinh \beta (1 - \cos \alpha \cosh \beta + \sin^2 \alpha)}{4(\cos \alpha - \cosh \beta)^3} + \frac{\alpha\beta^2 \sin \alpha (1 - \cos \alpha \cosh \beta - \sinh^2 \beta)}{2(\cos \alpha - \cosh \beta)^3},$$

$$(4.19) \quad G_{12}(\alpha, \beta) = -\frac{\pi\alpha(1 - \cos \alpha \cosh \beta)}{2(\cos \alpha - \cosh \beta)^2} - \frac{\pi\alpha\beta \sinh \beta (1 - \cos \alpha \cosh \beta + \sin^2 \alpha)}{2(\cos \alpha - \cosh \beta)^3}.$$

and

$$(4.20) \quad G_{13}(\alpha, \beta) = \\ -\frac{\pi \sin \alpha}{2} \left( \frac{1}{\cos \alpha - \cosh \beta} + \frac{3\beta \sinh \beta}{(\cos \alpha - \cosh \beta)^2} - \frac{\beta^2(1 - \cos \alpha \cosh \beta - \sinh^2 \beta)}{(\cos \alpha - \cosh \beta)^3} \right).$$

Detailed derivation for Eq. (4.16) is listed in Appendix A. It has been found a posteriori that the internal resolved shear stress components accounting for the pair density evolution come from  $\mathcal{O}(1/N)$ . Thus unless specified, the expansions to all resolved shear stresses will be truncated at  $o(1/N)$ , where  $o$  means ‘‘smaller than the order of’’. To ensure this accuracy, we further choose

$$(4.21) \quad K \sim \sqrt{N}.$$

Analogically,  $\hat{\tau}_{\text{int}}^{\text{in}}(\hat{q}_n, \hat{s})$  is asymptotically calculated by

$$(4.22) \quad \hat{\tau}_{\text{int}}^{\text{in}}(\hat{q}_n, \hat{s}) \sim (\pi\phi'_n) \cdot G_0(2\pi\zeta_n\phi'_n, 2\pi S\phi'_n) + \frac{2\zeta_n\phi'_n}{K} - \frac{\zeta_n\phi'_n}{K^2} \\ + \frac{\phi''_n}{N\phi'_n} \cdot G_{11}(2\pi\zeta_n\phi'_n, 2\pi S\phi'_n) + \frac{(\zeta_n\phi'_n)'}{N} \cdot G_{12}(2\pi\zeta_n\phi'_n, 2\pi S\phi'_n) \\ + \frac{\phi'_n\zeta'_n}{N} \cdot G_{13}(2\pi\zeta_n\phi'_n, 2\pi S\phi'_n) + o\left(\frac{1}{N}\right).$$

**4.2. Outer region approximation.** For  $\hat{x}_j$  belonging to the outer region, the expansion given by Eq. (4.12) may not hold since  $(j-n)/N$  can grow as large as  $\mathcal{O}(1)$ . However, according to Eq. (4.3), we have

$$(4.23) \quad \frac{K}{N} < |\phi(\hat{x}_n) - \phi(\hat{x}_j)| = \phi'(c_0)|\hat{x}_n - \hat{x}_j|,$$

where  $c_0$  takes some value between  $\hat{x}_j$  and  $\hat{x}_n$ . Eq. (4.23) suggests that

$$(4.24) \quad |\hat{x}_j - \hat{x}_n| \gg 1/N,$$

for all  $\hat{x}_j \in \Omega_{\text{out}}^n$ . Eq. (4.24) implies that the distance between the centre of a dislocation pair associated with  $\Omega_{\text{out}}^n$  to  $\hat{x}_n$  is much larger compared to the spacing between neighbouring dislocation pairs. Based on such findings, it takes two steps to find the expansion of the resolved shear stress at  $(\hat{p}_n, 0)$  due to the  $j$ -th pair, which is actually the  $j$ -th term in the sum appearing in Eq. (4.6). First, we relate  $\hat{p}_j$  and  $\hat{q}_j$  to  $\hat{x}_j$ , and relate  $\hat{p}_n$  and  $\hat{q}_n$  to  $\hat{x}_n$  by using Eq. (3.9) or (3.10). Then we can perform the expansion with reference to Eq. (4.24).

Following these two steps, the resolved shear stress at  $(\hat{p}_n, 0)$  due to the  $j$ -th pair is asymptotically calculated by

$$(4.25) \quad \begin{aligned} \frac{1}{N} \cdot \left( \frac{1}{\hat{p}_n - \hat{p}_j} - \frac{(\hat{p}_n - \hat{q}_j)((\hat{p}_n - \hat{q}_j)^2 - (S/N)^2)}{((\hat{p}_n - \hat{q}_j)^2 + (S/N)^2)^2} \right) &\sim -\frac{1}{N^2} \cdot \frac{\zeta_j}{(\hat{x}_n - \hat{x}_j)^2} \\ &+ \frac{1}{N^3} \cdot \frac{\zeta_n \zeta_j - 3S^2}{(\hat{x}_n - \hat{x}_j)^3} + \frac{1}{N^4} \cdot \frac{3\zeta_j(6S^2 - \zeta_n^2) + 18S^2\zeta_n - \zeta_j}{4(\hat{x}_j - \hat{x}_n)^4} + \mathcal{O}\left(\frac{1}{K^5}\right). \end{aligned}$$

It is implied from Eq. (4.25) that the leading order effect of the stress at  $(\hat{p}_n, 0)$  due to the positive dislocation at  $(\hat{p}_j, 0)$  cancels with that due to its pair partner located at  $(\hat{q}_n, \hat{s})$ .

It is worth noting that, when the truncation is made,  $1/|\hat{x}_j - \hat{x}_n|$  can be as large as  $\mathcal{O}(N/K)$ . Besides, the summation made for outer region approximation involves almost  $N$  terms. Therefore, to ensure an accuracy of  $o(1/N)$  for a resolved stress component, which results from a summation over almost  $N$  terms, the truncation made at each term in the summation should be at  $o(1/N^2)$ . This is the reason that a truncation at  $\mathcal{O}(1/K^5)$  is made in Eq. (4.25), where  $K \sim \sqrt{N}$ .

Based on Eq. (4.25), the expansion of  $\hat{\tau}_{\text{int}}^{\text{out}}(\hat{p}_n, 0)$  is obtained as

$$(4.26) \quad \begin{aligned} \hat{\tau}_{\text{int}}^{\text{out}}(\hat{p}_n, 0) &\sim -\frac{1}{N^2} \cdot \sum_{\substack{0 \leq j < n-K \\ n+K < j \leq N}} \frac{\zeta_j}{(\hat{x}_n - \hat{x}_j)^2} + \frac{1}{N^3} \cdot \sum_{\substack{0 \leq j < n-K \\ n+K < j \leq N}} \frac{\zeta_n \zeta_j - 3S^2}{(\hat{x}_n - \hat{x}_j)^3} \\ &+ \frac{1}{N^4} \cdot \sum_{\substack{0 \leq j < n-K \\ n+K < j \leq N}} \frac{3\zeta_j(6S^2 - \zeta_n^2) + 18S^2\zeta_n - \zeta_j}{4(\hat{x}_j - \hat{x}_n)^4} + \mathcal{O}\left(\frac{N}{K^5}\right) \end{aligned}$$

To evaluate the summations appearing in Eq. (4.26), one may make use of the Euler-Maclaurin formula. As detailed in Appendix B, we finally obtain the expansion of  $\hat{\tau}_{\text{int}}^{\text{out}}(\hat{p}_n, 0)$  by

$$(4.27) \quad \begin{aligned} \hat{\tau}_{\text{int}}^{\text{out}}(\hat{p}_n, 0) &\sim \frac{2}{K} \cdot (\zeta_n \phi'_n) - \frac{1}{K^2} \cdot \zeta_n \phi'_n + \frac{1}{N} \cdot \left( \frac{\phi'_0 \zeta_0}{\hat{x}_n - \hat{x}_0} - \frac{\phi'_N \zeta_N}{\hat{x}_n - \hat{x}_N} \right) \\ &+ \frac{1}{N} \int_{\hat{x}_0}^{\hat{x}_N} \frac{(\phi'(a)\zeta(a))' da}{\hat{x}_n - a} + o\left(\frac{1}{N}\right), \end{aligned}$$

where the integral is evaluated in the sense of principle value. In a similar way, we find that

$$(4.28) \quad \hat{\tau}_{\text{out}}(\hat{q}_n, \hat{s}) \sim \hat{\tau}_{\text{out}}(\hat{p}_n, 0) + o(1/N).$$

**4.3. Total resolved shear stress.** Now we put the results from the inner expansion by Eq. (4.16) and from the outer expansion by (4.27) together to obtain the expansion of  $\hat{\tau}_{\text{int}}(\hat{p}_n, 0)$  as

$$(4.29) \quad \begin{aligned} \hat{\tau}_{\text{int}}(\hat{p}_n, 0) &\sim (\pi\phi'_n) \cdot G_0(2\pi\phi_n\zeta_n, 2\pi S\phi'_n) + \frac{1}{N} \cdot \left( \frac{\phi'_0\zeta_0}{\hat{x}_n - \hat{x}_0} - \frac{\phi'_N\zeta_N}{\hat{x}_n - \hat{x}_N} \right) \\ &+ \frac{1}{N} \int_{\hat{x}_0}^{\hat{x}_N} \frac{(\phi'(a)\zeta(a))' da}{\hat{x}_n - a} - \frac{\phi''_n}{N\phi'_n} \cdot G_{11}(2\pi\phi'_n\zeta_n, 2\pi S\phi'_n) \\ &- \frac{(\phi'_n\zeta_n)'}{N} \cdot G_{12}(2\pi\phi'_n\zeta_n, 2\pi S\phi'_n) - \frac{\phi''_n\zeta'_n}{N} \cdot G_{13}(2\pi\phi'_n\zeta_n, 2\pi S\phi'_n) + o\left(\frac{1}{N}\right). \end{aligned}$$

It is worth noting that the  $\mathcal{O}(1/K)$  and  $\mathcal{O}(1/K^2)$  terms from the inner expansion cancel with their counterparts from the outer expansion. As a result, no trace of the intermediate parameter  $K$  is seen in Eq. (4.29).

In a similar way, we get the expansion of  $\hat{\tau}_{\text{int}}(\hat{q}_n, 0)$

$$(4.30) \quad \begin{aligned} \hat{\tau}_{\text{int}}(\hat{q}_n, \hat{s}) &\sim (\pi\phi'_n) \cdot G_0(2\pi\phi_n\zeta_n, 2\pi S\phi'_n) + \frac{1}{N} \cdot \left( \frac{\phi'_0\zeta_0}{\hat{x}_n - \hat{x}_0} - \frac{\phi'_N\zeta_N}{\hat{x}_n - \hat{x}_N} \right) \\ &+ \frac{1}{N} \int_{\hat{x}_0}^{\hat{x}_N} \frac{(\phi'(a)\zeta(a))' da}{\hat{x}_n - a} + \frac{\phi''_n}{N\phi'_n} \cdot G_{11}(2\pi\phi'_n\zeta_n, 2\pi S\phi'_n) \\ &+ \frac{(\phi'_n\zeta_n)'}{N} \cdot G_{12}(2\pi\phi'_n\zeta_n, 2\pi S\phi'_n) + \frac{\phi''_n\zeta'_n}{N} \cdot G_{13}(2\pi\phi'_n\zeta_n, 2\pi S\phi'_n) + o\left(\frac{1}{N}\right). \end{aligned}$$

Accordingly the external stress  $\hat{\tau}_{\text{ext}}$  at  $(\hat{p}_n, 0)$  can also be expanded near  $(\hat{x}_n, 0)$

$$(4.31) \quad \hat{\tau}_{\text{ext}}(\hat{p}_n, 0) \sim \hat{\tau}_{\text{ext}}^0(\hat{x}_n) - \frac{\zeta_n^{(0)}}{2N} \cdot \frac{\partial \hat{\tau}_{\text{ext}}^0(\hat{x}_n)}{\partial \hat{x}} + o\left(\frac{1}{N}\right),$$

where for simplicity

$$(4.32) \quad \hat{\tau}_{\text{ext}}^0(\hat{x}) := \hat{\tau}_{\text{ext}}(\hat{x}_n, 0), \quad \frac{\partial \hat{\tau}_{\text{ext}}^0(\hat{x})}{\partial \hat{x}} := \frac{\partial \hat{\tau}_{\text{ext}}(\hat{x}, 0)}{\partial \hat{x}}.$$

Similarly,

$$(4.33) \quad \hat{\tau}_{\text{ext}}(\hat{q}_n, \hat{s}) \sim \hat{\tau}_{\text{ext}}^0(\hat{x}_n) + \frac{1}{N} \left( \frac{\zeta_n^{(0)}}{2} \cdot \frac{\partial \hat{\tau}_{\text{ext}}^0(\hat{x}_n)}{\partial \hat{x}} + S \cdot \frac{\partial \hat{\tau}_{\text{ext}}^0(\hat{x}_n)}{\partial \hat{y}} \right) + o\left(\frac{1}{N}\right),$$

where

$$(4.34) \quad \frac{\partial \hat{\tau}_{\text{ext}}^0(\hat{x})}{\partial \hat{y}} = \frac{\partial \hat{\tau}_{\text{ext}}(\hat{x}, 0)}{\partial \hat{y}}.$$

Here  $\partial \hat{\tau}_{\text{ext}}^0/\partial \hat{x}$  and  $\partial \hat{\tau}_{\text{ext}}^0/\partial \hat{y}$  may be considered as the ‘‘stress gradients’’, which capture the difference in the externally applied stress field due to spatial variation within a pair of dipole.

Therefore, the total resolved shear stress at  $(\hat{p}_n, 0)$  is expressed by

$$\begin{aligned}
(4.35) \quad \hat{\tau}_{\text{tot}}(\hat{p}_n, 0) &\sim (\pi\phi'_n) \cdot G_0(2\pi\phi_n\zeta_n, 2\pi S\phi'_n) + \hat{\tau}_{\text{ext}}^0(\hat{x}_n) \\
&+ \frac{1}{N} \cdot \left( \frac{\phi'_0\zeta_0}{\hat{x}_n - \hat{x}_0} - \frac{\phi'_N\zeta_N}{\hat{x}_n - \hat{x}_N} \right) + \frac{1}{N} \int_{\hat{x}_0}^{\hat{x}_N} \frac{(\phi'(a)\zeta(a))' da}{\hat{x}_n - a} \\
&- \frac{\phi''_n}{N\phi'_n} \cdot G_{11}(2\pi\phi'_n\zeta_n, 2\pi S\phi'_n) - \frac{(\phi'_n\zeta_n)'}{N} \cdot G_{12}(2\pi\phi'_n\zeta_n, 2\pi S\phi'_n) \\
&- \frac{\phi''_n\zeta'_n}{N} \cdot G_{13}(2\pi\phi'_n\zeta_n, 2\pi S\phi'_n) - \frac{\zeta^{(0)}}{2N} \frac{\partial \hat{\tau}_{\text{ext}}^0(\hat{x}_n)}{\partial \hat{x}} + o\left(\frac{1}{N}\right),
\end{aligned}$$

where it is recalled that  $G_0$ ,  $G_{11}$ ,  $G_{12}$  and  $G_{13}$  are defined by Eqs. (4.17) - (4.20). Similarly,

$$\begin{aligned}
(4.36) \quad \hat{\tau}_{\text{tot}}(\hat{q}_n, 0) &\sim (\pi\phi'_n) \cdot G_0(2\pi\phi_n\zeta_n, 2\pi S\phi'_n) + \hat{\tau}_{\text{ext}}^0(\hat{x}_n) \\
&+ \frac{1}{N} \cdot \left( \frac{\phi'_0\zeta_0}{\hat{x}_n - \hat{x}_0} - \frac{\phi'_N\zeta_N}{\hat{x}_n - \hat{x}_N} \right) + \frac{1}{N} \int_{\hat{x}_0}^{\hat{x}_N} \frac{(\phi'(a)\zeta(a))' da}{\hat{x}_n - a} \\
&+ \frac{\phi''_n}{N\phi'_n} \cdot G_{11}(2\pi\phi'_n\zeta_n, 2\pi S\phi'_n) + \frac{(\phi'_n\zeta_n)'}{N} \cdot G_{12}(2\pi\phi'_n\zeta_n, 2\pi S\phi'_n) \\
&+ \frac{\phi''_n\zeta'_n}{N} \cdot G_{13}(2\pi\phi'_n\zeta_n, 2\pi S\phi'_n) + \frac{\zeta_n^{(0)}}{2N} \cdot \frac{\partial \hat{\tau}_{\text{ext}}^0(\hat{x}_n)}{\partial \hat{x}} + \frac{S}{N} \cdot \frac{\partial \hat{\tau}_{\text{ext}}^0(\hat{x}_n)}{\partial \hat{y}} + o\left(\frac{1}{N}\right).
\end{aligned}$$

**5. Dislocation dynamical model at the continuum level.** In this section, we derive for the governing equation for the two field variables  $\phi$  and  $\zeta$  at the continuum level. Here we first consider the continuous description for the equilibrium states, where the total resolved shear stress at each dislocation vanishes.

**5.1. Governing equations for the equilibrium states.** When all dipoles rest in force balance, the total resolved shear stress  $\hat{\tau}_{\text{tot}}(\hat{p}_n, 0)$  and  $\hat{\tau}_{\text{tot}}(\hat{q}_n, \hat{s})$  should be zero for all  $n$  according to the law of motion governed by Eq. (3.1) and (3.2). It is worth noting that since the resulting equation for  $\phi$  and  $\zeta$  are established in an asymptotic sense, we also need to expand  $\phi$  and  $\zeta$  by

$$(5.1) \quad \phi(\hat{t}, \hat{x}) \sim \phi^{(0)}(\hat{t}, \hat{x}) + \frac{\phi^{(1)}(\hat{t}, \hat{x})}{N} + \dots$$

and

$$(5.2) \quad \zeta(\hat{t}, \hat{x}) \sim \zeta^{(0)}(\hat{t}, \hat{x}) + \frac{\zeta^{(1)}(\hat{t}, \hat{x})}{N} + \dots,$$

respectively. Substituting the above expansions into Eqs. (4.35) and (4.36) gives

$$\begin{aligned}
(5.3) \quad \hat{\tau}_{\text{tot}}(\hat{p}_n, \hat{s}) &\sim \left( \pi(\phi_n^{(0)})' \right) \cdot G_0(2\pi(\phi_n^{(0)})'\zeta_n^{(0)}, 2\pi S(\phi_n^{(0)})') + \hat{\tau}_{\text{ext}}^0(\hat{x}_n) \\
&+ \frac{1}{N} \cdot \left( \hat{\tau}_a^n - \hat{\tau}_b^n + \frac{\zeta_n^{(0)}}{2} \cdot \frac{\partial \hat{\tau}_{\text{ext}}^0(\hat{x}_n)}{\partial \hat{x}} \right) + o\left(\frac{1}{N}\right)
\end{aligned}$$

and

$$\begin{aligned}
(5.4) \quad \hat{\tau}_{\text{tot}}(\hat{q}_n, \hat{s}) &\sim \left( \pi(\phi_n^{(0)})' \right) \cdot G_0(2\pi(\phi_n^{(0)})'\zeta_n^{(0)}, 2\pi S(\phi_n^{(0)})') + \hat{\tau}_{\text{ext}}^0(\hat{x}_n) \\
&+ \frac{1}{N} \cdot \left( \hat{\tau}_a^n + \hat{\tau}_b^n + \frac{\zeta_n^{(0)}}{2} \cdot \frac{\partial \hat{\tau}_{\text{ext}}^0(\hat{x}_n)}{\partial \hat{x}} + S \cdot \frac{\partial \hat{\tau}_{\text{ext}}^0(\hat{y}_n)}{\partial \hat{x}} \right) + o\left(\frac{1}{N}\right),
\end{aligned}$$

respectively, where for simplicity

$$(5.5) \quad \hat{\tau}_a^n := \frac{\phi_0' \zeta_0^{(0)}}{\hat{x}_n - \hat{x}_0} - \frac{(\phi_N^{(0)})' \zeta_N^{(0)}}{\hat{x}_n - \hat{x}_N} + \int_{\hat{x}_0}^{\hat{x}_n} \frac{(\phi'(a) \zeta(a)^{(0)})' dt}{\hat{x}_n - t} \\ + \zeta_n^{(1)} \frac{\partial G_0(2\pi(\phi_n^{(0)})' \zeta_n^{(0)}, 2\pi S(\phi_n^{(0)})')}{\partial \zeta_n^{(0)}} + (\phi_n^{(1)})' \frac{\partial G_0(2\pi(\phi_n^{(0)})' \zeta_n^{(0)}, 2\pi S(\phi_n^{(0)})')}{\partial (\phi_n^{(0)})'}$$

and

$$(5.6) \quad \hat{\tau}_b^n := \frac{(\phi_n^{(0)})''}{(\phi_n^{(0)})'} \cdot G_{11}(2\pi(\phi_n^{(0)})' \zeta_n^{(0)}, 2\pi S(\phi_n^{(0)})') \\ + ((\phi_n^{(0)})' \zeta_n^{(0)})' \cdot G_{12}(2\pi(\phi_n^{(0)})' \zeta_n^{(0)}, 2\pi S(\phi_n^{(0)})') \\ + (\phi_n^{(0)})'' (\zeta_n^{(0)})' \cdot G_{13}(2\pi(\phi_n^{(0)})' \zeta_n^{(0)}, 2\pi S(\phi_n^{(0)})').$$

Now letting the right hand side of Eq. (5.3) and (5.4) vanish, we asymptotically obtain one equation (associated with  $n$ ) from the leading order,  $\mathcal{O}(1)$ ,

$$(5.7) \quad \pi(\phi_n^{(0)})' \cdot G_0(2\pi(\phi_n^{(0)})' \zeta_n^{(0)}, 2\pi S(\phi_n^{(0)})') + \hat{\tau}_{\text{ext}}^0(\hat{x}_n) = 0$$

and two equations (associated with  $n$ ) from the next order,  $\mathcal{O}(1/N)$ ,

$$(5.8) \quad \hat{\tau}_a^n - \hat{\tau}_b^n - \frac{\zeta_n^{(0)}}{2} \cdot \frac{\partial \hat{\tau}_{\text{ext}}^0(\hat{x}_n)}{\partial \hat{x}} = 0$$

and

$$(5.9) \quad \hat{\tau}_a^n + \hat{\tau}_b^n + \frac{\zeta_n^{(0)}}{2} \cdot \frac{\partial \hat{\tau}_{\text{ext}}^0(\hat{x}_n)}{\partial \hat{x}} + S \cdot \frac{\partial \hat{\tau}_{\text{ext}}^0(\hat{y}_n)}{\partial \hat{x}} = 0$$

There are  $4(N+1)$  unknowns  $\{\phi_n^{(0)}\}_{n=0}^N$ ,  $\{\phi_n^{(1)}\}_{n=0}^N$ ,  $\{\zeta_n^{(0)}\}_{n=0}^N$  and  $\{\zeta_n^{(1)}\}_{n=0}^N$  in the above system consisting of  $3(N+1)$  equations. Hence we still need higher-order expansions to complete the equation systems. However, since we are mostly interested in the leading order effects of  $\phi_n$  and  $\zeta_n$ , we can subtract Eq. (5.9) by (5.8) to eliminate  $\zeta_n^{(1)}$  and  $\phi_n^{(1)}$ , both of which only appear in  $\tau_a^n$ , and then obtain

$$(5.10) \quad 2\hat{\tau}_b^n + \zeta_n^{(0)} \cdot \frac{\partial \hat{\tau}_{\text{ext}}^0(\hat{x}_n)}{\partial \hat{x}} + S \cdot \frac{\partial \hat{\tau}_{\text{ext}}^0(\hat{y}_n)}{\partial \hat{y}} = 0,$$

Eqs. (5.7) and (5.10) form a set of equations with  $2(N+1)$  unknowns  $\{\phi_n^{(0)}\}_{n=0}^N$  and  $\{\zeta_n^{(0)}\}_{n=0}^N$  to determine. Here we simply drop the superscript “ $(0)$ ”, because only the leading-order effects are taken into account.

Now we turn the obtained equations valid only at every  $\hat{x}_n$  to field equations valid for all  $\hat{x}$ . This can be achieved by using the fact that  $\hat{x}_n$  is densely distributed in the domain. Therefore, we drop the index  $n$  to re-write Eq. (5.7) and (5.10) by

$$(5.11) \quad \frac{\pi \phi' \sin(2\pi \phi' \zeta)}{\cosh(2\pi S \phi') - \cos(2\pi \phi' \zeta)} \cdot \left( 1 - \frac{2\pi S \phi' \sinh(2\pi S \phi')}{\cosh(2\pi S \phi') - \cos(2\pi \phi' \zeta)} \right) + \hat{\tau}_{\text{ext}}^0 = 0$$

and

$$(5.12) \quad 0 = \frac{2\phi''}{\phi'} \cdot G_{11}(2\pi \phi' \zeta, 2\pi S \phi') + 2(\phi' \zeta)' \cdot G_{12}(2\pi \phi' \zeta, 2\pi S \phi') \\ + 2(\phi'(\zeta)') \cdot G_{13}(2\pi \phi' \zeta, 2\pi S \phi') + \zeta \frac{\partial \hat{\tau}_{\text{ext}}^0}{\partial \hat{x}} + S \frac{\partial \hat{\tau}_{\text{ext}}^0}{\partial \hat{y}},$$

respectively, where it is recalled that  $G_{11}$ ,  $G_{12}$  and  $G_{13}$  are defined by Eqs. (4.18) - (4.20). Eqs. (5.11) and (5.12) are the two equations for the two field variables  $\phi$  and  $\zeta$  derived at the continuum level when the row of dipoles rest in their equilibrium states. It is worth noting that Eq. (5.11) comes from the leading order force balance and Eq. (5.12) comes from the difference in the force balance equations obtained from the next order.

**5.2. Governing equations for the dynamical relations.** Now we consider reformulating the discrete dislocation dynamics governed by Eqs. (3.1) to (3.4) at the continuum level.

According to the dislocation mobility law given by Eq. (3.1), the  $n$ -th positive dislocation can be tracked by

$$(5.13) \quad \frac{d\hat{p}_n}{d\hat{t}} = \hat{\tau}_{\text{tot}}(\hat{p}_n, 0)$$

Analogically, we have

$$(5.14) \quad \frac{d\hat{q}_n}{d\hat{t}} = -\hat{\tau}_{\text{tot}}(\hat{q}_n, \hat{s}).$$

Then we look for the evolution equations for  $\phi$  and  $\zeta$ . We know that  $\phi(\hat{t}, \hat{x}_n(\hat{t})) = n/N$  by definition at any time  $\hat{t}$ . Thus taking the derivative with respect to  $\hat{t}$  on both sides of it gives rise to

$$(5.15) \quad \frac{\partial \phi_n}{\partial \hat{t}} + \frac{d\hat{x}_n}{d\hat{t}} \cdot \frac{\partial \phi_n}{\partial \hat{x}} = 0.$$

According to the definition of  $\hat{x}_n$  given by Eq. (3.7), we have

$$(5.16) \quad \frac{d\hat{x}_n}{d\hat{t}} = \hat{\tau}_{\text{tot}}(\hat{p}_n, 0) - \hat{\tau}_{\text{tot}}(\hat{q}_n, \hat{s})$$

where Eqs. (5.13) and (5.14) are employed. With the asymptotic expansions for  $\hat{\tau}_{\text{tot}}(\hat{p}_n, 0)$  and  $\hat{\tau}_{\text{tot}}(\hat{q}_n, \hat{s})$  given by Eqs (4.35) and (4.36), respectively, we can incorporate Eq. (5.16) into (5.15) to get

$$(5.17) \quad \begin{aligned} & \frac{\partial \phi_n}{\partial \hat{t}} - \frac{1}{N} \left( \frac{2\phi_n''}{\phi_n'} G_{11}(2\pi\phi_n'\zeta_n, 2\pi S\phi_n') + 2(\phi_n'\zeta_n)' G_{12}(2\pi\phi_n'\zeta_n, 2\pi S\phi_n') \right) \frac{\partial \phi_n}{\partial \hat{x}} \\ & - \frac{1}{N} \left( 2(\phi_n'\zeta_n)' G_{13}(2\pi\phi_n'\zeta_n, 2\pi S\phi_n') + \zeta \frac{\partial \hat{\tau}_{\text{ext}}^0(\hat{x}_n)}{\partial \hat{x}} + S \frac{\partial \hat{\tau}_{\text{ext}}^0(\hat{x}_n)}{\partial \hat{y}} \right) \frac{\partial \phi_n}{\partial \hat{x}} \sim o\left(\frac{1}{N}\right). \end{aligned}$$

Again we can drop the subscript  $n$  to rewrite Eq. (5.17) as an differential equation valid for all  $\hat{x}$  by

$$(5.18) \quad \frac{\partial \phi}{\partial \hat{t}} - \frac{1}{N} \left( 2\hat{\tau}_b + \zeta \cdot \frac{\partial \hat{\tau}_{\text{ext}}^0}{\partial \hat{x}} + S \cdot \frac{\partial \hat{\tau}_{\text{ext}}^0}{\partial \hat{y}} \right) \cdot \frac{\partial \phi}{\partial \hat{x}} \sim o\left(\frac{1}{N}\right),$$

where for simplicity

$$(5.19) \quad \hat{\tau}_b := \frac{\phi''}{\phi'} G_{11}(2\pi\phi'\zeta, 2\pi S\phi') + (\phi'\zeta)' G_{12}(2\pi\phi'\zeta, 2\pi S\phi') + \phi'\zeta' G_{13}(2\pi\phi'\zeta, 2\pi S\phi').$$

Eq. (5.18) can be considered as the evolution equation for  $\phi$  in an asymptotical sense.

It can be seen from Eq. (5.18) that the evolution speed of  $\phi$  is as small as  $\mathcal{O}(1/N)$ . This suggests that the actual time scale associated with the evolution of  $\phi$ , the dislocation pair density potential, is characterised by a slow-varying temporal variable given by

$$(5.20) \quad \hat{t}_s = N\hat{t}.$$

With Eq. (5.20) and taking the leading order effect of Eq. (5.18), we get the evolution equation for  $\phi$  to be

$$(5.21) \quad \frac{\partial \phi}{\partial \hat{t}_s} - \left( 2\hat{\tau}_b + \zeta \frac{\partial \hat{\tau}_{\text{ext}}^0}{\partial \hat{x}} + S \frac{\partial \hat{\tau}_{\text{ext}}^0}{\partial \hat{y}} \right) \cdot \frac{\partial \phi}{\partial \hat{x}} = 0$$

On the other hand, according to the definition of  $\zeta$  by Eq. (3.6), we have

$$(5.22) \quad \frac{\partial \zeta_n}{\partial \hat{t}} + \frac{d\hat{x}_n}{d\hat{t}} \cdot \frac{\partial \zeta_n}{\partial \hat{x}} = \frac{d\zeta_n(\hat{t}, \hat{x}(\hat{t}))}{d\hat{t}} = N \cdot \left( \frac{d\hat{q}_n}{d\hat{t}} - \frac{d\hat{p}_n}{d\hat{t}} \right).$$

Combining Eqs. (4.35), (4.36), (5.13), (5.14), (5.16) and (5.22) then dropping the subscript  $n$ , we asymptotically derive an equation for  $\zeta$  as

$$(5.23) \quad \frac{\partial \zeta}{\partial \hat{t}} \sim \frac{2N\pi\phi' \sin(2\pi\phi'\zeta)}{\cosh(2\pi S\phi') - \cos(2\pi\phi'\zeta)} \left( \frac{2\pi S\phi' \sinh(2\pi S\phi')}{\cosh(2\pi S\phi') - \cos(2\pi\phi'\zeta)} - 1 \right) - 2N\hat{\tau}_{\text{ext}}^0 + \mathcal{O}(1).$$

It is seen from Eq. (5.23) that  $\zeta$  evolves as fast as  $\mathcal{O}(N)$ . This means  $\zeta$  should be studied at a fast temporal scale characterised by

$$(5.24) \quad \hat{t}_f = \frac{\hat{t}}{N}$$

Then the equation for  $\zeta$  is obtained by

$$(5.25) \quad \frac{\partial \zeta}{\partial \hat{t}_f} = - \frac{2\pi\phi' \sin(2\pi\phi'\zeta)}{\cosh(2\pi S\phi') - \cos(2\pi\phi'\zeta)} \cdot \left( 1 - \frac{2\pi S\phi' \sinh(2\pi S\phi')}{\cosh(2\pi S\phi') - \cos(2\pi\phi'\zeta)} \right) - 2\hat{\tau}_{\text{ext}}^0.$$

The discrepancy in the evolving speeds of  $\zeta$  and  $\phi$  can be interpreted as follows. When observed at the time scale characterised by  $\hat{t}_s$ , at which  $\phi$  evolves normally, the evolution of  $\zeta$  takes place too quickly to be felt by  $\phi$  before the steady state is reached. This means when the evolution of  $\phi$  is considered, we only need to take into account the steady state solution of Eq. (5.25) at each time slot  $\hat{t}_s$ , that is,

$$(5.26) \quad \frac{\pi\phi' \sin(2\pi\phi'\zeta)}{\cosh(2\pi S\phi') - \cos(2\pi\phi'\zeta)} \cdot \left( 1 - \frac{2\pi S\phi' \sinh(2\pi S\phi')}{\cosh(2\pi S\phi') - \cos(2\pi\phi'\zeta)} \right) + \hat{\tau}_{\text{ext}}^0 = 0,$$

which is effectively the leading order force balance equation (5.11).

Therefore, the dynamical relation of a row of dislocation dipoles at the continuum model can be described by an equilibrium equation (5.26) for  $\zeta$  and an evolution equation (5.21) for  $\phi$ , and the time scale associated with the resulting model is characterised by the slow time scale variable  $\hat{t}_s$ .

**6. Equilibria at the continuum level.** In this section, we will analyse the equilibrium states at the continuum level determined by Eqs. (5.11) and (5.12). We will begin with the case where the externally applied stress is almost diminishing. In this case, two types of possibly stable configurations out of three are found as a result of the force balance equation at the leading order and a natural transition between different equilibrium patterns is seen as due to instability. At the next order, the detailed equations for  $\phi$  and  $\zeta$  corresponding to various equilibrium states will be finally derived. The analytical results will then be validated through comparison with the numerical solutions to the same problem. In the end of this section, we will analyse the case under an external applied stress, which is arbitrarily given.

**6.1. Equilibria under an almost vanishing external stress field.** Since it is still complicated to analyse Eq. (5.11) and (5.12), we start with a simple case where the externally applied resolved shear stress almost vanishes, i.e.

$$(6.1) \quad \hat{\tau}_{\text{ext}}^0 = 0.$$

Here we say this is the almost-vanishing-external-stress case because the stress gradients  $\partial\hat{\tau}_{\text{ext}}^0/\partial\hat{x}$  and  $\partial\hat{\tau}_{\text{ext}}^0/\partial\hat{y}$  do not have to be 0.

**6.1.1. Implication from the leading-order force balance equation.** With Eq. (6.1), the leading order force balance equation (5.11) becomes

$$(6.2) \quad \frac{\sin(2\pi\phi'\zeta)}{\cosh(2\pi S\phi') - \cos(2\pi\phi'\zeta)} \cdot \left(1 - \frac{2\pi S\phi' \sinh(2\pi S\phi')}{\cosh(2\pi S\phi') - \cos(2\pi\phi'\zeta)}\right) = 0.$$

Eq. (6.2) can be regarded as an implicit relation between two quantities  $\phi'\zeta$  and  $\phi'S$ . In fact, these two quantities are physically meaningful. It is recalled that the pair density  $\phi'$  can be approximated by the reciprocal of the spacing between two neighbouring pair centers scaled by  $N$  and  $S$  is the slip plane gap rescaled by  $N$  according to Eq. (3.5),  $\phi'S$  effectively captures the ratio of slip plane gap to the spacing of neighbouring pairs. Also since  $\zeta/N$  is the pair width at  $\hat{x}$  according to Eq. (3.6),  $\phi'\zeta$  measures how the pair width is compared with the spacing of neighbouring pairs.

From Eq. (6.2), there are three possible choices for  $\zeta$  as functions of  $\phi'$  and other parameters.

- Equilibrium Type I when  $\zeta = 0$ . The corresponding microstructure is shown in Fig. 4(a). Within each dislocation pair, the positive and the negative dislocations are vertically aligned.
- Equilibrium Type II when  $\phi'\zeta = 1/2$ . The corresponding microstructure is shown in Fig. 4(b). Since  $\phi'\zeta$  represents the ratio of pair width to pair center spacing,  $\phi'\zeta = 1/2$  suggests that every negative dislocation lies roughly in the middle of its two neighbouring positive dislocations. We term the equilibrium of this type as a “non-localised” structure, because each dislocation is “shared” by its two neighbours (of opposite sign).
- Equilibrium Type III when

$$(6.3) \quad \zeta = \frac{1}{2\pi\phi'} \cos^{-1}(\cosh(2\pi S\phi') - 2\pi S\phi' \sinh(2\pi S\phi')).$$

The corresponding microstructure is shown in Fig 4(c). A positive dislocation here is bonded with a negative one to form a real dipole, and the equilibrium of this type is named as a “localised structure”.

It is worth noting that Eq. (6.3) only holds when

$$(6.4) \quad -1 \leq \cosh(2\pi S\phi') - 2\pi S\phi' \sinh(2\pi S\phi') \leq 1,$$

which numerically gives rise to a range for  $S\phi'$  by

$$(6.5) \quad 0 \leq S\phi' \leq 0.2465.$$

Hence the emergence of Equilibrium Type III is conditional.

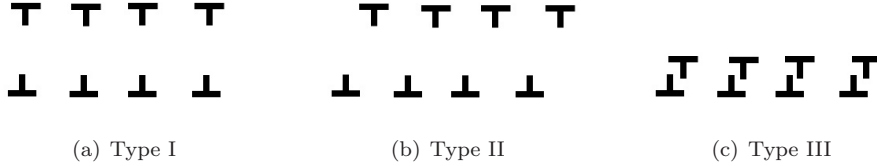


FIG. 4. *Three types of equilibria: (a)  $\zeta = 0$ ; (b)  $\zeta\phi' = 1/2$  with non-localised structures formed; (c)  $\zeta$  satisfies Eq. (6.3) and localised structures are formed.*

Actually, if we set  $X = \phi'\zeta$  and  $Y = \phi'S$ , the configuration becomes a row of dipoles periodic in  $X$ , which have been studied by [20]. Thus the stability of the obtained three types of equilibria can be examined by employing the same arguments proposed by [20] and we draw the following conclusions

- Equilibrium Type I ( $\zeta = 0$ ), it is always unstable.
- Equilibrium Type II ( $\phi'\zeta = 1/2$ ), it is only stable when Equilibrium Type III do not exist.
- Equilibrium Type III ( $\zeta$  satisfies Eq. (6.3)), it is always stable as long as it exists.

Another way to investigate the stability of the obtained equilibrium states is to consider the strain energy per unit length denoted by  $E/L$  with respect to  $\zeta$ . Since  $\zeta/N$  denotes the dipole width, for an infinitesimal change in  $\zeta$ , the resulting change in strain energy per unit length should satisfy

$$(6.6) \quad d\left(\frac{E}{L}\right) = \frac{b\hat{\tau}_{\text{int}}^{(0)}}{2} \cdot \frac{d\zeta}{N},$$

with reference to the idea of defining elastic strain energy of a straight dislocation detailed in [12]. Integrating Eq. (6.6) with respect to  $\zeta$  gives rise to

$$(6.7) \quad \frac{E}{L} = \frac{\log(\cosh(2\pi S\phi') - \cos(2\pi\zeta\phi'))}{4\pi\phi'N} + \frac{S \sinh(2\pi S\phi')}{2N(\cosh(2\pi S\phi') - \cos(2\pi\zeta\phi'))},$$

where the constant coming from integration is set to be 0. Theoretically, a stable equilibrium state should correspond to a local minimum of  $E/L$ .

The energy per length rescaled by  $1/(2N\phi')$  against  $\zeta$  for different  $\phi'S$  are shown in Fig. 5. It is seen from Fig. 5(a) that when condition (6.5) is not satisfied, there are two equilibrium states, and Equilibrium Type II is the stable one. When condition (6.5) is met, we have got three equilibrium states as shown in Fig. 5, and Equilibrium Type III is the stable one.

Here a natural transition from a non-localised structure (Type II) to a localised structure (Type III) takes place as the slip plane spacing gets narrower. Such transition may be indicative to the formation of the persistent slip bands, and further discussion over this issue will be made in §8.2.

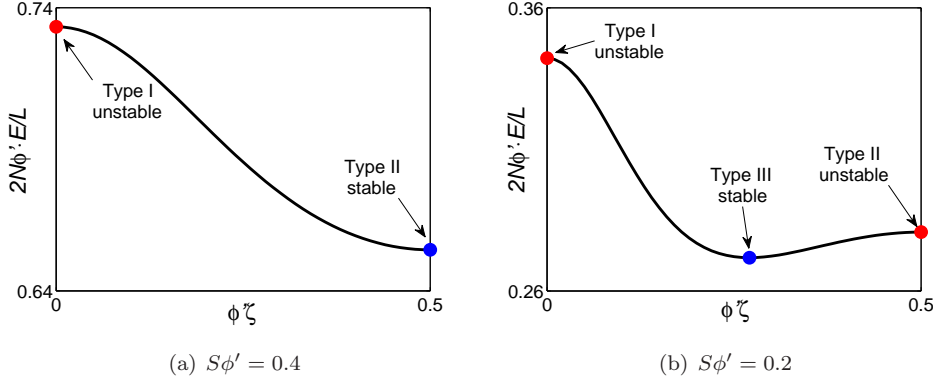


FIG. 5. A stable equilibrium state should correspond to  $\zeta\phi'$ , which minimises the strain energy per length (rescaled by  $1/(2N\phi')$ ). (a) If  $S\phi'$  is larger than 0.2465, only two types of equilibria exist and Type II is the stable configuration. (b) If  $0 < S\phi' < 0.2465$ , a transition in stability from Type II to Type III takes place.

**6.1.2. Next order equation for Equilibrium Type II.** Based on the solutions to the leading order equation (5.7), we now investigate the next order force balance equation (5.10). Here only stable configurations, i.e. Equilibrium Type II and III, are considered.

When  $\phi'\zeta = 1/2$  (Type II), one can make use of the fact that  $(\phi'\zeta)' = 0$  and  $\sin(2\pi\phi'\zeta) = 0$ . This suggests that the terms associated with  $G_{12}$  and  $G_{13}$  in Eq. (5.10) both vanish. Therefore, the equation for  $\phi'$  can be obtained as

$$\begin{aligned}
 0 &= \frac{2\phi''}{\phi'} \cdot G_{11}(\pi, 2\pi S\phi') + \frac{1}{2\phi'} \cdot \frac{\partial \hat{\tau}_{\text{ext}}^0}{\partial \hat{x}} + S \frac{\partial \hat{\tau}_{\text{ext}}^0}{\partial \hat{y}} \\
 (6.8) \quad &= -\frac{\phi''}{\phi'} - 4\pi S\phi'' \tanh(\pi S\phi') + 5\pi^2 S^2 \phi' \phi'' \text{sech}^2(\pi S\phi') \\
 &\quad - 2\pi^3 S^3 (\phi')^2 \phi'' \text{sech}^2(\pi S\phi') \tanh(\pi S\phi') + \frac{1}{2\phi'} \cdot \frac{\partial \hat{\tau}_{\text{ext}}^0}{\partial \hat{x}} + S \frac{\partial \hat{\tau}_{\text{ext}}^0}{\partial \hat{y}}.
 \end{aligned}$$

Eq. (6.8) is a differential equation of  $\phi'$ . Its solution describes the pair density distribution in equilibrium when all dipoles form non-local structures as shown in Fig. 4(b).

To justify our results for  $\phi'$  and  $\zeta$  calculated from the continuum model, we also consider the equilibrium states obtained by the discrete dislocation dynamical model, which is the reference model. To do that, we simply put  $N + 1$  pairs of dipoles in the domain  $[0, 1]$  and let the system evolve to the steady state following Eqs. (3.1) - (3.4). The temporal derivatives needed for DDD simulations are approximated by using the Euler scheme with time step  $\Delta t_{\text{dis}}$  chosen by

$$(6.9) \quad \Delta t_{\text{dis}} = \frac{0.025}{N}.$$

For all simulation results presented in this paper, we lock one dislocation at each end. For example, at the left boundary, we set  $\hat{p}_0 = 0$ . There is strict requirement for  $\hat{q}_0$ , except  $\hat{q}_0 \geq 0$ . Similarly at the right end, we set  $\hat{q}_N = 1$  and let  $\hat{p}_N < 1$ . By doing this, the total number of dislocation pairs are conserved during the simulation.

Correspondingly at the continuum level, this condition is translated by

$$(6.10) \quad \int_0^1 \phi'(\hat{t}, \hat{x}) d\hat{x} = \phi(\hat{t}, 1) - \phi(\hat{t}, 0) = 1.$$

Now we compare the results for Equilibrium Type II obtained from the continuum and the discrete models. For simplicity, we consider the case when  $\partial \hat{\tau}_{\text{ext}}^0 / \partial \hat{x} = 0$  and  $\partial \hat{\tau}_{\text{ext}}^0 / \partial \hat{y}$  is a constant. Thus we can integrate Eq. (6.8) on both sides to obtain

$$(6.11) \quad \log\left(\frac{\cosh(\pi\phi'S)}{\phi'}\right) + \left(\frac{\pi\phi'S}{\cosh(\pi\phi'S)}\right)^2 + 3\pi\phi'S \tanh(\pi\phi'S) = C - \frac{\partial \hat{\tau}^0}{\partial \hat{y}} \cdot S\hat{x},$$

where  $C$  is a constant to be determined by using condition (6.10).

We begin with the case where no stress gradient is applied to the system, i.e.  $\partial \hat{\tau}_{\text{ext}}^0 / \partial \hat{x} = \partial \hat{\tau}_{\text{ext}}^0 / \partial \hat{y} = 0$ . Eq. (6.11) suggests  $\phi' = 1$  and we then obtain  $\zeta = 1/2$ . This means that in the absence of applied stress gradients, all dipoles are uniformly distributed and the dipoles from non-localised structures suggested by the continuum model. To see Equilibrium Type II from the discrete dislocation dynamical model, one needs a relative large  $S$ , which is chosen to be 0.3 here. It is noted that in the discrete model, the pair density is approximated by

$$(6.12) \quad \rho_{\text{dis}}((\hat{p}_n + \hat{q}_n)/2) = \frac{1}{N(\hat{p}_{n+1} - \hat{p}_n)}$$

and  $\zeta$  is approximated by

$$(6.13) \quad \zeta_{\text{dis}}((\hat{p}_n + \hat{q}_n)/2) = N(\hat{q}_n - \hat{p}_n).$$

A comparison of the values of  $\phi'$  and  $\zeta$  from the discrete and the continuum models is shown in Fig. 6 and good agreement between the two models is seen except near the boundaries. In fact, there exists a boundary layer near each end, where the results

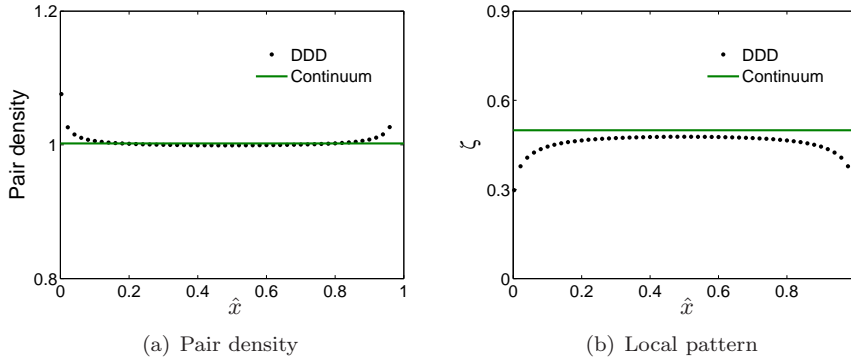


FIG. 6. Comparison of the pair density and the pair width Equilibrium Type II with the results from the discrete dislocation dynamical models under no externally applied stress. When  $S = 0.3$ , dipoles form Equilibrium Type II. Here  $N = 50$ .

from the continuum model deviate from its DDD counterpart. This is because the symmetry required for the setting up of the inner region  $\Omega_{\text{in}}^n$  given by Eq. (4.2) breaks down. As a result, the intermediate parameter  $K$  can not be eliminated at the leading

order. This means the force balance equations should be set up in a new regime near the boundaries. However, as seen later, if we increase the total number  $N$ , which brings up the effective length of the domain, the influence of this boundary layer effect gets weakened away from the two ends. One way to reduce the deviation near the two ends is to apply the techniques devised in [16], and it is not in the scope of this paper.

When the system is applied a non-vanishing stress-gradient, for example,  $\partial\hat{\tau}^0/\partial\hat{y} = 1$ , one can again calculate  $\phi'$  and  $\zeta$  with reference to Eq. (6.11). The results from the two models are compared in Fig. 7 and excellent agreement is seen again away from the two ends.

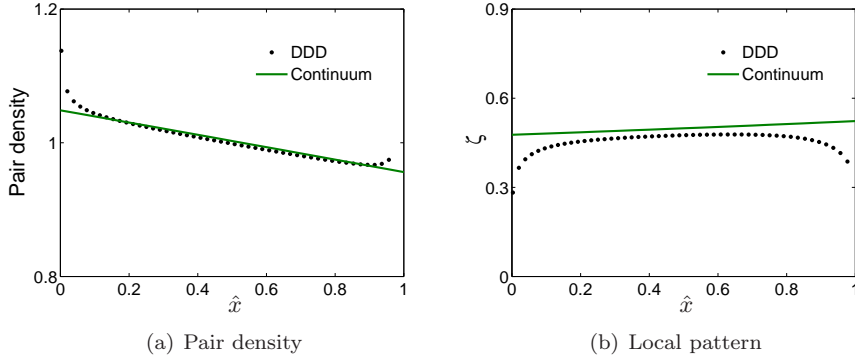


FIG. 7. When the system is applied an stress gradient  $\partial\hat{\tau}^0/\partial\hat{y} = 1$ , the dipoles of Equilibrium Type II are seen piling-up against the left boundary. Here  $S = 0.3$  and  $N = 50$ .

### 6.1.3. Next order force balance equation for Equilibrium Type III.

Analogically, we can study the next order equation (5.10), when all dipoles are in Equilibrium Type III, i.e. condition (6.5) is met. To do that, we first update  $G_{11}$ ,  $G_{12}$  and  $G_{13}$  respectively defined by (4.18) to (4.20) and we obtain

$$\begin{aligned}
 (6.14) \quad G_{11}^{III} &= G_{11}(\cos^{-1}(\cosh(2\pi S\phi') - 2\pi S\phi' \sinh(2\pi S\phi')), 2\pi S\phi') \\
 &= \frac{\text{csch}^2(2\pi S\phi')}{8} ((1 - (2\pi S\phi')^2)(1 - \cosh(4\pi S\phi')) + 4\pi S\phi' \sinh(4\pi S\phi')) \\
 &\quad - \frac{\sqrt{2}\zeta \cosh(2\pi S\phi') \sqrt{4\pi S\phi' \sinh(4\pi S\phi') - (1 + (2\pi S\phi')^2) \sinh^2(4\pi S\phi')}}{4},
 \end{aligned}$$

$$\begin{aligned}
 (6.15) \quad G_{12}^{III} &= G_{12}(\cos^{-1}(\cosh(2\pi S\phi') - 2\pi S\phi' \sinh(2\pi S\phi')), 2\pi S\phi') \\
 &= - \frac{\zeta \text{csch}(2\pi S\phi') ((1 + (2\pi S\phi')^2) \sinh(2\pi S\phi') - 4\pi S\phi' \cosh(2\pi S\phi'))}{8\pi (S\phi')^2}
 \end{aligned}$$

and

$$\begin{aligned}
 (6.16) \quad G_{13}^{III} &= G_{13}(\cos^{-1}(\cosh(2\pi S\phi') - 2\pi S\phi' \sinh(2\pi S\phi')), 2\pi S\phi') \\
 &= - \frac{\pi \coth(2\pi S\phi') \sqrt{2\pi S\phi' \sinh(4\pi S\phi') - (1 + (2\pi S\phi')^2) \sinh^2(2\pi S\phi')}}{2}.
 \end{aligned}$$

Then we substitute  $G_{11}$ ,  $G_{12}$  and  $G_{13}$  in Eq. (5.10) respectively by  $G_{11}^{III}$ ,  $G_{12}^{III}$  and  $G_{13}^{III}$  and we thus derive an equation for  $\phi'$  as

$$(6.17) \quad 0 = \frac{2\pi S^2 \phi' \phi'' \cosh(2\pi S \phi')}{\sqrt{2\pi S \phi' \sinh(4\pi S \phi') - (1 + (2\pi S \phi')^2) \sinh^2(2\pi S \phi')}} \cdot (G_{12}^{III} + G_{13}^{III}) + \frac{2\phi''}{\phi'} \cdot G_{11}^{III} - \frac{\phi'' \zeta}{2\pi(\phi')^2} \cdot G_{13}^{III} + \frac{1}{2\phi'} \cdot \frac{\partial \hat{\tau}_{\text{ext}}^0}{\partial \hat{x}} + S \frac{\partial \hat{\tau}_{\text{ext}}^0}{\partial \hat{y}}.$$

Since the above equation for  $\phi'$  is too complicated to analyse, we wish to find simple but representative expressions for  $\phi'$  and  $\zeta$ . Recalling from condition (6.5) that Equilibrium Type III only appears for small  $\phi' S$ , we can consider the asymptotic behaviour of the above equation as  $S \rightarrow 0$ . Physically, this means the two slip planes are close to each other.

When  $S$  is small, one can asymptotically solve Eq. (6.3) to get

$$(6.18) \quad \zeta \approx S + \frac{2(\pi\phi')^2 S^3}{3}.$$

Eq. (6.18) implies that the pair width in this case is almost the same as the slip plane gap. When these two quantities are identical, we call this structure a 45° dipole. In fact, a 45° dipole is the stable configuration of an isolated pair of dipole. As from Eq. (6.18), when the two slip planes get close to each other, the mutual interaction between the pair partners become dominant over the stresses due to all other dislocations and the dipoles appear similar as isolated dipolar pairs. Incorporating Eq. (6.18) into the next order equation (5.10), we can asymptotically derive an equation for the pair density  $\phi'$  as

$$(6.19) \quad 2\pi^2 S^2 \phi' \phi'' + S \cdot \left( \frac{\partial \hat{\tau}_{\text{ext}}^0}{\partial \hat{x}} + \frac{\partial \hat{\tau}_{\text{ext}}^0}{\partial \hat{y}} \right) = 0.$$

Eqs. (6.18) and (6.19) are the equations for  $\phi'$  and  $\zeta$  when  $S \rightarrow 0$ . Compared to the original equations given by (6.3) and (6.17), they enjoy much simpler forms. Now we compare their solutions to DDD simulation results to show they can be used as alternative governing equations for Equilibrium Type III at the continuum level.

Here we still consider the case when  $\partial \hat{\tau}_{\text{ext}}^0 / \partial \hat{x} = 0$  and  $\partial \hat{\tau}_{\text{ext}}^0 / \partial \hat{y}$  is a constant for simplicity. Hence the pair density distribution  $\phi'$  can be solved from Eq. (6.19)

$$(6.20) \quad \phi' = \frac{1}{\pi S} \sqrt{C - \frac{\partial \hat{\tau}^0}{\partial \hat{y}} \cdot S \hat{x}},$$

where  $C$  is determined by the boundary condition (6.10).

We first investigate the case with no applied stress gradient. From Eq. (6.20), we obtain  $\phi' = 1$  and  $\zeta$  is calculated to be 0.1066 from Eq. (6.18). We then compare these results with that from the DDD simulations in Fig. 8. Excellent agreement between the two models is visualised. Here we find again that in the absence of applied stress gradient, the dipoles are uniformly distributed.

Now we consider a non-vanishing applied stress gradient set to be  $\partial \hat{\tau}^0 / \partial \hat{y} = 1$ . By using Eqs. (6.18) and (6.19), we can plot  $\phi'$  and  $\zeta$  against  $\hat{x}$  in Fig. 9 and they are shown agreeing well with the outcomes from the underlying DDD model. The comparison results shown above suggest that we can use Eqs. (6.18) and (6.19) to describe the collective behaviour of a row of dislocation dipoles forming Equilibrium of Type III.

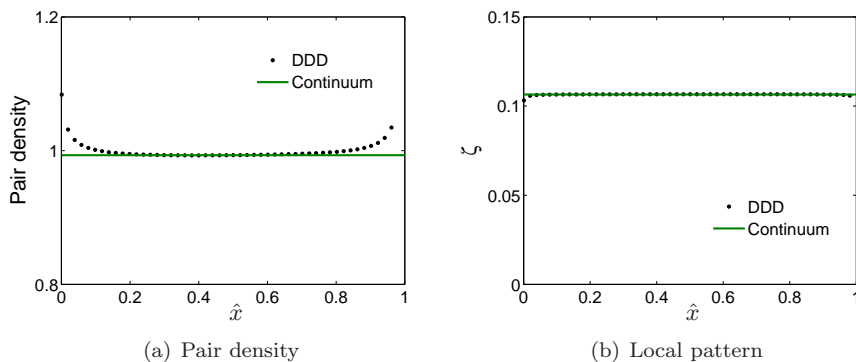


FIG. 8. Comparison of results from the continuum and the DDD models for the case where there is no applied stress gradient. When  $S = 0.1$ , the system takes the equilibrium state of Type III with  $\phi' \approx 1$  and  $\zeta \approx 0.1066$ . Here  $N = 50$ .

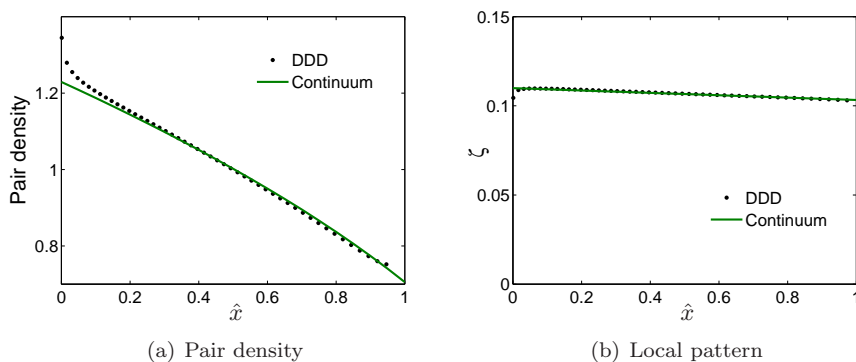


FIG. 9. Dipoles of Equilibrium Type III are found piling-up against an applied stress gradient to the left boundary. Here  $S = 0.1$ ,  $\partial\tau^0/\partial\hat{y} = 1$  and  $N = 50$ .

**6.1.4. Equilibria of mixed types.** According to Eq. (6.5),  $\phi'S = 0.2465$  characterises the transition between Equilibrium Type II and III. Therefore, when the value of  $\phi' - 0.2465/S$  changes its sign, the continuum model suggests a change in equilibrium patterns. This can also be observed by setting  $S = 0.24$  in Fig. 10. Here  $N$  is chosen to be 100. From Fig. 10 that Type II and III co-exist at equilibrium states. Near the left boundary, the dipoles take Equilibrium Type II and a transition from Type II to III is found taking place away from the left boundary. The derived continuum model suggests that the transition should happen when

$$(6.21) \quad \phi' = \frac{0.2465}{S} \approx 1.03,$$

which gives rise to the dashed line in Fig. 10. It can be checked that the Equilibrium Type III roughly emerges, where  $\phi'$  drops below the dashed line. In Fig. 10, it can also be seen that the values of the pair density agree well with each for both cases, while there is roughly a 10% variance in  $\zeta$  for Equilibrium Type II. It is seen later that a rising  $N$  will bring down the deviation in  $\phi'$  and  $\zeta$  from their reference data produced from the DDD model.

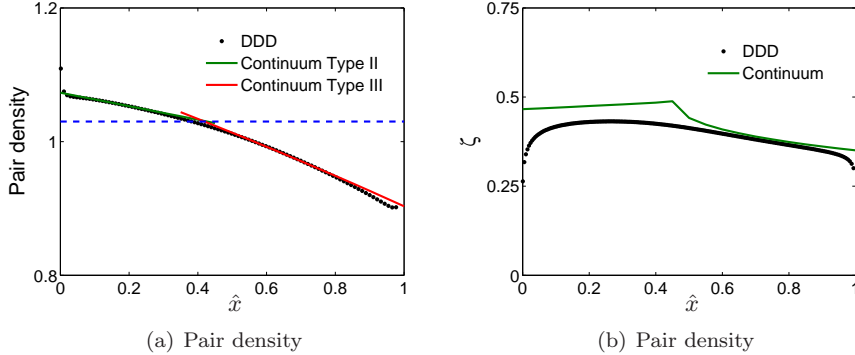


FIG. 10. When  $S = 0.24$ , Equilibrium Type II and III are found co-exist. Near the left boundary, the dipoles take the equilibrium of Type II. A natural transition from Type II to III is seen roughly where the pair density drops below the dashed line characterised by Eq. (6.21). Here  $N = 100$ .

**6.1.5. Summary.** To summarise, a row of dipoles may form two types of stable equilibria if the applied stress is almost-vanishing. When  $\phi'S \geq 0.2465$ , the resulting equations at the continuum level of the pair density  $\phi'$  and (rescaled) pair width  $\zeta$  are derived to be Eq. (6.8) and  $\zeta = 1/(2\phi')$ . When  $0 < \phi'S < 0.2465$ , the collective behaviour of a row of dipoles can be approximately described by Eqs. (6.18) and (6.19).

**6.2. Equilibria under arbitrary externally-applied stresses.** Now we generalise our discussion to the case where the leading order of the external resolved shear stress is non-vanishing, i.e.  $\tau_{\text{ext}}^0 \sim \mathcal{O}(1)$ . In this case, Eq. (5.11) may not be solved explicitly. However, some analysis can still be done to understand the resulting equilibrium configurations.

If we use the expression of  $G_0$  defined by Eq. (4.17), we can rewrite Eq. (5.11) by

$$(6.22) \quad G_0(2\pi\phi'\zeta, 2\pi\phi'S) + \frac{\tau_{\text{ext}}^0}{\pi\phi'} = 0.$$

Eq. (6.22) describes the inter-relation of three quantities,  $\zeta\phi'$ ,  $S\phi'$  and  $\hat{\tau}_{\text{ext}}^0/\pi$  and we can define

$$(6.23) \quad X = \zeta\phi', \quad Y = S\phi', \quad \Upsilon = \frac{\hat{\tau}_{\text{ext}}^0}{\pi\phi'}$$

to facilitate further analysis. As discussed in §6.1.1,  $X$  and  $Y$  measures respectively the pair width and the slip plane gap, both scaled by the spacing between the neighbouring dipolar centers. By using Eq. (6.23), we rewrite Eq. (6.22) by

$$(6.24) \quad -G_0(2\pi X, 2\pi Y) = \Upsilon.$$

Eq. (6.24) suggests that the inter-relation between  $X$  and  $Y$  for a given  $\Upsilon$  can be visualised by the contours of  $-G_0(2\pi X, 2\pi Y)$  as shown in Fig. 11. It can be observed from Fig. 11 that there exists a  $Y^*$  (attained at  $X^*$  say) such that  $Y \leq Y^*$  on each contour. To calculate this  $Y^*$ , one may differentiate Eq. (6.24) along the contour characterised by  $\Upsilon$  and we obtain

$$(6.25) \quad \frac{\partial G_0(2\pi X, 2\pi Y)}{\partial X} + \frac{\partial G_0(2\pi X, 2\pi Y)}{\partial Y} \cdot \frac{dY}{dX} = 0,$$

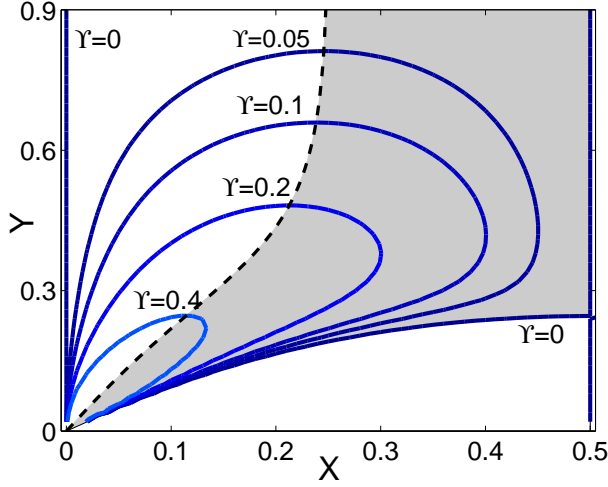


FIG. 11. Given any  $\Upsilon$ , a pair of  $(X, Y)$ , which satisfies Eq. (6.24) should sit on the contour  $-G_0(2\pi\phi'\zeta, 2\pi\phi'S)$  with height  $\Upsilon$ . For each  $\Upsilon$ , there exists a  $Y^*$  (attained at  $X^*$  say) such that  $Y \leq Y^*$ . The locus of such  $(X^*, Y^*)$  lies on the dashed curve which is drawn with reference to Eq. (6.26). For any  $Y < Y^*$  (under a given  $\Upsilon$ ), there are two possible values for  $X$ . Only those  $(X, Y)$  falling in the shaded region correspond to stable configurations.

where  $dY/dX$  is the tangent of the contour at  $(X, Y)$ . If  $Y$  takes its maximum value at  $Y^*$ , then  $dY/dX$  should vanish there. Thus Eq. (6.25) becomes

$$(6.26) \quad 0 = \frac{\cos(2\pi X^*)}{\cosh(2\pi Y^*) - \cos(2\pi X^*)} \cdot \left( 1 - \frac{2\pi Y^* \sinh(2\pi Y^*)}{\cosh(2\pi Y^*) - \cos(2\pi X^*)} \right) - \frac{\sin^2(2\pi X^*)}{(\cosh(2\pi Y^*) - \cos(2\pi X^*))^2} + \frac{4\pi Y^* \sin^2(2\pi X^*) \sinh(2\pi Y^*)}{(\cosh(2\pi Y^*) - \cos(2\pi X^*))^3},$$

where the expression for  $G_0$  in Eq. (4.17) is employed. Based on Eq. (6.26), the locus of the point  $(X^*, Y^*)$  with  $\Upsilon$  varying should lie on the dashed curve in Fig. 11.

It can also be observed from Fig. 11 that there exist two choices for  $X$  when any  $Y < Y^*$  and the larger one gives rise to a stable equilibrium state according to numerics. Therefore, only those  $(X, Y)$  falling into the shaded region in Fig. 11 correspond to stable configurations.

It is worth noting that here  $\Upsilon > 0$  is considered in the analysis presented above. When  $\Upsilon < 0$ , we simply let  $X < 0$  and same conclusion will be drawn.

The above analysis provides us some insight to the equilibrium configurations. Nevertheless, to find  $\zeta$  and  $\phi'$  satisfying Eq. (5.11) and (5.12), one has to turn to numerical methods. In fact, it will be seen that the equilibrium solutions for  $\zeta$  and  $\phi'$  are effectively the steady state solutions to the dynamical equations given by Eqs (5.21) and (5.26).

## 7. Comparison of the continuum model with its underlying DDD model.

Now we compare the simulation results obtained by applying the derived continuum model and the DDD model to same dynamical processes. For simulations at the discrete level, the set-ups and procedures are taken in a same manner as in §6.1.2. To numerically implement the derived continuum model, we discretise Eqs. (5.21) and

(5.26) with  $\Delta x$  in space and  $\Delta t_{\text{con}}$  in time. At each time step, we take the following procedure to update the two variables  $\phi$  and  $\zeta$ . With  $\phi$  computed from the previous step, we can (numerically) solve Eq. (5.26) to update the values for  $\zeta$  at each spatial grid point. It is worth noting that following the analysis in §6.2, one need to ensure the computed  $\zeta$  is associated with a stable equilibrium state. Then we can use Eq. (5.21) to compute  $\phi$ . The Courant-Friedrichs-Lewy (CFL) condition is needed when discretising Eq. (5.21). This is because Eq. (5.21) is actually of (non-linear) parabolic type. For simulation results presented in this paper, we used  $\Delta t_{\text{con}} = 1.25\Delta x^2$ .

Our goal here is to check the accuracy and the efficiency of the derived continuum model with reference to its underlying DDD model. To measure accuracy, we define

$$(7.1) \quad \text{Err}_{\phi'} = \max_{\hat{x} \in I} \frac{\phi' - \rho_{\text{dis}}}{\rho_{\text{dis}}},$$

where  $\rho_{\text{dis}}$  denotes the density computed by the DDD simulations;  $I = [0.1, 0.9]$  to avoid the generic deviation between the two methods near the two boundaries. Thus  $\text{Err}_{\phi'}$  can be used as a measurement of the relative error of the pair density caused by the discrete-to-continuum transition. In a similar sense, we define a measurement to the relative error of the pair width by

$$(7.2) \quad \text{Err}_{\zeta} = \max_{\hat{x} \in I} \frac{\zeta - \zeta_{\text{dis}}}{\zeta_{\text{dis}}}.$$

The parameters chosen for the first set of numerical examples are  $S = 0.3$ ,  $N = 50$ ,  $\hat{\tau}_{\text{ext}}^0 = 0.5$  and  $\partial \hat{\tau}_{\text{ext}}^0 / \partial \hat{y} = 1$ . In Table. 1,  $\text{Err}_{\phi'}$  and  $\text{Err}_{\zeta}$  at various time slots are listed. It is seen that the relative errors in the pair density at different stages are no

$\hat{t}$	1	2	5	10	20	26.4
$\text{Err}_{\phi'}$	0.0229	0.0217	0.0161	0.0094	0.0078	0.0079
$\text{Err}_{\zeta}$	0.0807	0.0812	0.0815	0.0817	0.0818	0.0818

TABLE 1

Defined by Eq. (7.1),  $\text{Err}_{\phi'}$  provides a measurement to the relative error of the pair density caused by the discrete-to-continuum transition. Similarly  $\text{Err}_{\zeta}$  given by Eq. (7.2) provides a measurement to the relative error of the pair width  $\zeta/N$ . Here  $S = 0.3$ ,  $\hat{\tau}_{\text{ext}}^0 = 0.5$ ,  $\partial \hat{\tau}_{\text{ext}}^0 / \partial \hat{y} = 1$  and  $N = 50$ .  $\text{Err}_{\phi'}$  and  $\text{Err}_{\zeta}$  are listed at various time slots.

more than 2.5%, while the relative errors in pair width are roughly 8%. In Fig. 12, snap shots of pair density by DDD and the continuum methods at  $\hat{t} = 1, 5, 10$  and 20 are shown.

Then we also check the efficiency of the derived continuum model by keeping all other parameters unchanged while increasing the total number  $N$ . For this purpose, we introduce two quantities  $T_{\text{con}}$  and  $T_{\text{dis}}$ , which denote the actual time it takes a simulation to reach the steady states by using the continuum and DDD model, respectively. Thus  $T_{\text{con}}/T_{\text{dis}}$  becomes a measurement to the computational efficiency of using the continuum model against its underlying DDD model. The smaller this value is, the higher efficiency the continuum model displays.

It is worth noting that  $N$  has been scaled off in the continuum model. Hence an increase in  $N$  only affects the outcomes of the DDD models.

The comparison results between the two models for different  $N$  are collected in Fig. 13. In Fig. 13(a),  $T_{\text{con}}/T_{\text{dis}}$  is found scaling with  $N$  at an exponent of roughly  $-3.25$ . It can be checked that when the total number of dislocation pairs is increased

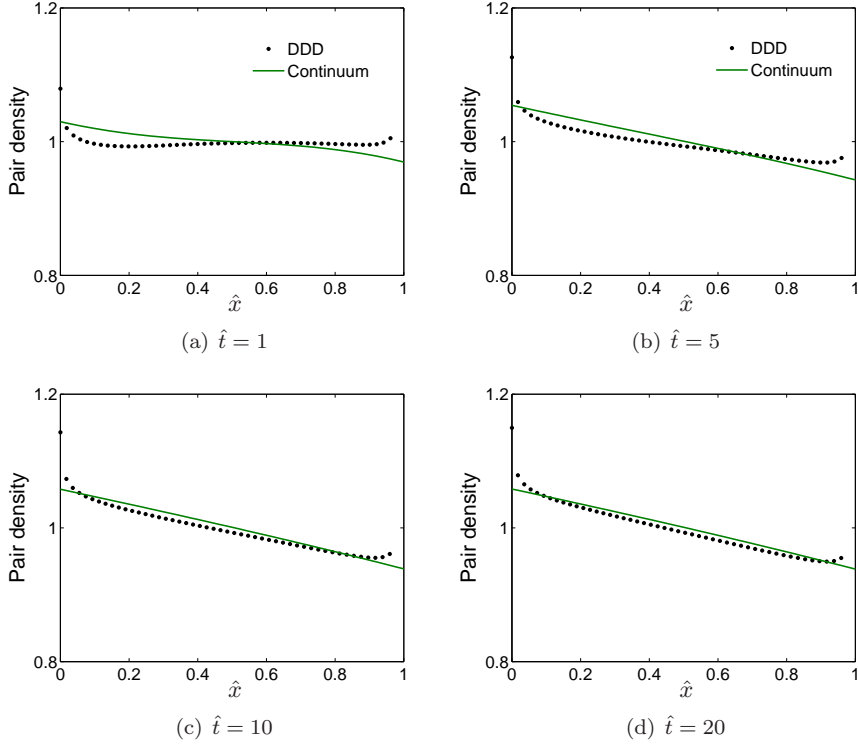


FIG. 12. Snap shots of the pair density obtained from the DDD and the continuum methods at  $\hat{t} = 1, 5, 10$  and  $20$ .

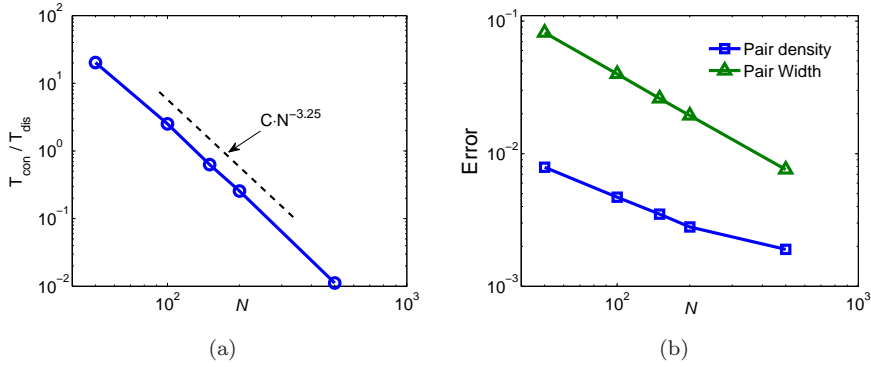


FIG. 13. (a)  $T_{\text{con}}/T_{\text{dis}}$  provides a measurement to the computational efficiency exhibited by the continuum model compared to its underlying DDD model. The smaller this value is, the more efficient the continuum model is. (b) The upscaling errors of the pair density  $\phi'$  and the pair width as the systems attain their steady states with various  $N$ .

to 500, the time it takes for the continuum model to reach the steady state is roughly 1% of that needed for the DDD model. The rationalisation of the exponent  $-3.25$  is as follows. For DDD simulation, it roughly takes a time of  $\mathcal{O}(N^2)$  to compute the pair-interaction among  $2N$  particles at each step. This along with  $\mathcal{O}(N)$  steps needed

to reach the equilibrium states (estimated with reference to Eq. (6.9)) adds up to an actual computational time at  $\mathcal{O}(N^3)$  and this gives rise to an exponent of almost  $-3$ .

To check the upscaling accuracy of the derived continuum model, we also plot  $\text{Err}_{\phi'}$  and  $\text{Err}_{\zeta}$  given by Eqs. (7.1) and (7.2), respectively against  $N$ . The coarse-graining errors for both quantities drop with an increasing  $N$  as shown in Fig. 13(b). When  $N$  is 500, the coarse graining error of  $\zeta$  becomes as good as no more than 1%. This is sensible since the continuum model is obtained through performing asymptotic analysis in terms of  $1/N$ . An increased  $N$  effectively brings down the truncation errors.

Moreover, the dynamical processes based on the two models are also compared for the case when  $S$  is as small as 0.1. In this scenario, the governing equations at the continuum level can be simplified as

$$(7.3) \quad \zeta \sim S - 2S^2 \hat{\tau}_{\text{ext}}^0 + \mathcal{O}(S^3),$$

and

$$(7.4) \quad \frac{\partial \phi}{\partial t_s} - \left( 2\pi^2 S^2 \phi'' \phi' + \zeta \cdot \frac{\partial \hat{\tau}_{\text{ext}}^0}{\partial \hat{x}} + S \cdot \frac{\partial \hat{\tau}_{\text{ext}}^0}{\partial \hat{y}} \cdot \frac{\partial \phi}{\partial \hat{x}} \right) \frac{\partial \phi}{\partial \hat{x}} = 0,$$

where the asymptotic behaviour for  $S \rightarrow 0$  is considered.

In Table 2, the coarse-graining errors for the pair density and the pair width are shown with  $N = 50$ .

$\hat{t}$	5	10	20	50	100	250
$\text{Err}_{\phi'}$	0.0238	0.0325	0.0445	0.0435	0.0135	0.0210
$\text{Err}_{\zeta}$	0.0612	0.0625	0.0660	0.0726	0.0775	0.0802

TABLE 2

The coarse-graining errors of the pair density distribution and the pair width at various time slots. Here  $S = 0.1$ ,  $\hat{\tau}^0 = 0.5$ ,  $\partial \hat{\tau}^0 / \partial \hat{y} = 1$ ,  $N = 50$ .

It can be shown from the comparison results presented above that, the dynamical equations (5.21) and (5.26) at the continuum level provide a good summary of its underlying DDD model in the sense of computational time saved and coarse-graining errors controlled at an acceptable level.

## 8. Conclusion and further discussion.

**8.1. Conclusion.** In this paper, we have studied the collective behaviour of a row of dislocation dipoles using matched asymptotic analysis. The discrete-to-continuum transition is facilitated by the introduction of two field variables, the dislocation pair density potential  $\phi$  and the dislocation pair width  $\zeta$ . The equilibrium states at the continuum level are governed by Eqs. (5.11) and (5.12), while the dynamical relations at the continuum level are formulated by Eqs (5.21) and (5.26). The following conclusions are drawn based on the analysis and the numerical implementation to the derived continuum model.

Dislocation dipoles are found ‘‘piling-up’’ against an externally applied stress gradient. In another word, the dislocation pairs are shown uniformly distributed in the absence of applied stress gradients.

When the externally applied stress is almost zero, we found three possible equilibrium patterns (as shown in Fig. 4), whose stability depends on the value of  $\phi'S$ , the ratio of the slip plane gap to the pair center spacing. If  $\phi'S$  is big (condition (6.5) breaks down), the non-localised structures (Equilibrium Type II) are the stable

configurations. While  $\phi'S$  falls below the critical value 0.2465, a localised equilibrium structure (Equilibrium Type III) emerges. In this scenario, Equilibrium Type II becomes unstable and a natural transition to Equilibrium Type III is observed.

If the externally applied shear stress  $\tau_{\text{ext}}^0$  is non-negligible, two possible equilibrium patterns are found and the one with larger pair width value corresponds to the stable configuration as suggested by the shaded region in Fig. 11.

With matched asymptotic analysis, the two introduced field variables are found evolving at speeds associated with different time scales. At the faster scale, the dislocation pairs rearrange themselves to reach a state of force balance established at the leading order. At the slower scale, the evolution of the pair density is found driven by the stress gradient, which comes from the next-order effect. Consequentially, the dipole dynamics, if viewed at the continuum level, can be modelled by an evolution equation for  $\phi$  given by Eq. (5.21) and an equilibrium equation for  $\zeta$  given by Eq. (5.26). All analytical results have been justified through comparison with the underlying DDD models.

**8.2. Implication to the formation of PSBs.** The transition from Equilibrium Type II to Type III, as suggested by our analysis, may shed light on understanding how localised persistent slip band structures emerge amid non-localised channel-vein structures. Nevertheless, the transition in equilibrium patterns due to instability found here may not provide a full explanation to the formation of PSBs, because the PSB walls consist more likely of several dislocation pairs rather than a single pair as indicated by the Equilibrium Type III. To further investigate the mechanism dictating the PSB formation, one may also need to study the stability of the pair density governed by Eq. (5.21). Another direction enlightened by our analysis is a further study of the role played by the externally applied stress gradients, which account for any non-uniformly distributed patterns according to our analytical results.

**8.3. Implication to incorporating SSDs into continuum models for plasticity.** The approaches here used to separate physical processes according to their associated time scales also provide us some hints to incorporating the statistically stored dislocations into continuum models of plasticity consistent with the underlying discrete dislocation dynamics. Given  $\hat{t}$  the time scale associated with the continuum model (termed as the continuum time scale), it has been shown that the mutual adjustment within dislocation pairs characterised by the evolution of  $\zeta$  takes place so fast that only the steady (equilibrium) states are observable at the continuum time scale. On the other hand, the evolution of the pair density potential  $\phi$  takes place so slowly that it appears static observed at the continuum time scale. Analogically, a well-established continuum model of plasticity is expected to be hierarchic in time. It should consist of a set of evolution equations for the geometrically necessary dislocations (GNDs) changing at a normal speed accompanied by another set of quasi-static equations describing the SSD structures in equilibrium.

**Appendix A. Expansion of  $\hat{\tau}_{\text{in}}^{\text{int}}(\hat{p}_n, 0)$ .** To find the asymptotic expansion of  $\hat{\tau}_{\text{in}}^{\text{int}}(\hat{p}_n, 0)$  defined by Eq. (4.5), we first use Eq. (4.14) to estimate  $1/(N(\hat{p}_n - \hat{p}_j))$

$$\begin{aligned} \frac{1}{N} \frac{1}{\hat{p}_n - \hat{p}_j} &\sim -\frac{\phi'_n}{j-n} - \frac{1}{N} \cdot \left( \frac{\zeta'_n}{2(j-n)} + \frac{\phi''_n}{2\phi'_n} \right) + \frac{j-n}{N^2} \cdot \left( \frac{(\phi''_n)^2}{4(\phi'_n)^3} - \frac{\phi'''_n}{6(\phi'_n)^2} \right) \\ &\quad - \frac{1}{4N^2} \cdot \left( \frac{\phi'_n(\zeta'_n)^2}{4(j-n)} + \frac{\zeta'_n\phi''_n}{\phi'_n} + \zeta''_n \right) + \mathcal{O}\left(\frac{K^2}{N^3}\right). \end{aligned} \tag{A.1}$$

It is worth noting that when making truncation to the above expansions, the order of magnitude of  $(j-n)$  may grow as large as  $K$ . Besides, it has been found as a posteriori that the internal resolved shear stresses accounting for the pair density evolution come from the next order of the expansion, i.e.  $\mathcal{O}(1/N)$ . Hence to ensure that the accuracy of the expansion in Eq. (A.1) meets this requirement, we need  $K \sim \sqrt{N}$ , which is Eq. (4.21).

With reference to Eq. (A.1), the first sum in Eq. (4.5) becomes

$$(A.2) \quad \frac{1}{N} \sum_{\substack{j=n-K \\ j \neq n}}^{n+K} \frac{1}{\hat{p}_n - \hat{p}_j} \sim -\frac{K}{N} \cdot \frac{\phi_n''}{\phi_n'} + \mathcal{O}\left(\frac{K^3}{N^3}\right).$$

It is noted that to derive for Eq. (A.2), symmetry in  $j-n$  from  $-K$  to  $K$  is employed.

Analogically, to prepare for evaluating the second sum in Eq. (4.5), we use Eqs. (4.14) and (4.15) to calculate

$$(A.3) \quad \begin{aligned} \frac{(\hat{p}_n - \hat{q}_j)((\hat{p}_n - \hat{q}_j)^2 - \hat{s}^2)}{((\hat{p}_n - \hat{q}_j)^2 + \hat{s}^2)^2} &\sim -\frac{\phi_n' \cdot (j-n + \phi_n' \zeta_n) \left( (j-n + \phi_n' \zeta_n)^2 - (S\phi_n')^2 \right)}{\left( (j-n + \phi_n' \zeta_n)^2 + (S\phi_n')^2 \right)^2} \\ &- \frac{\phi_n''}{N\phi_n'} \cdot \frac{(j-n)^2(j-n + \phi_n' \zeta_n)^4 - 6(j-n + \phi_n' \zeta_n)^2(S\phi_n')^2 + (S\phi_n')^4}{\left( (j-n + \phi_n' \zeta_n)^2 + (S\phi_n')^2 \right)^3} \\ &+ \frac{1}{N^2} \cdot \frac{(j-n + \phi_n' \zeta_n)^5(j-n)^4(\phi_n'')^2}{\left( (j-n + \phi_n' \zeta_n)^2 + (S\phi_n')^2 \right)^4(\phi_n')^3} \\ &- \frac{1}{N^2} \cdot \frac{(j-n + \phi_n' \zeta_n)^6(j-n)^3(3(\phi_n'')^2 - \phi_n''' \phi_n')}{6\left( (j-n + \phi_n' \zeta_n)^2 + (S\phi_n')^2 \right)^4(\phi_n')^3} + \mathcal{O}\left(\frac{K^2}{N^3}, \frac{1}{N^2}\right), \end{aligned}$$

where  $\hat{s} = S/N$  defined by Eq. (3.5) is used. It is worth noting that the expansion (A.3) only holds for the case where at least one of  $S$  and  $\zeta_n$  is not too small. Otherwise the expansion in Eq. (A.3) gets singular for  $j = n$ .

Adding the right hand side of Eq. (A.3) over  $j$  from  $n-K$  to  $n+K$  gives rise to the asymptotic expression of the second sum in Eq. (4.5)

$$(A.4) \quad \begin{aligned} -\frac{1}{N} \sum_{j=n-K}^{n+K} \frac{(\hat{p}_n - \hat{q}_j)((\hat{p}_n - \hat{q}_j)^2 - \hat{s}^2)}{((\hat{p}_n - \hat{q}_j)^2 + \hat{s}^2)^2} &\sim (\pi\phi_n') \cdot G_0(2\pi\zeta_n\phi_n', 2\pi S\phi_n') + \frac{2\zeta_n\phi_n'}{K} \\ &+ \frac{K\phi_n''}{N\phi_n'} - \frac{N(\zeta_n\phi_n')}{K^2} - \frac{\phi_n''}{N\phi_n'} G_{11}(2\pi\zeta_n\phi_n', 2\pi S\phi_n') - \frac{(\zeta_n\phi_n')'}{N} G_{12}(2\pi\zeta_n\phi_n', 2\pi S\phi_n') \\ &- \frac{\phi_n''\zeta_n'}{N} G_{13}(2\pi\zeta_n\phi_n', 2\pi S\phi_n') + o\left(\frac{1}{N}\right), \end{aligned}$$

where  $G_0$ ,  $G_{11}$ ,  $G_{12}$  and  $G_{13}$  are defined by Eqs. (4.17) to (4.20). It is worth noting that the properties of the Poly-Gamma functions (for details, see [1]) are used for the derivation of Eq. (A.4). Combining Eqs. (A.2) and (A.4), we get the expansion for  $\hat{\tau}_{\text{in}}^{\text{int}}$  as given by Eq. (4.16).

**Appendix B. Expansion of  $\hat{\tau}_{\text{out}}^{\text{int}}(\hat{p}_n, 0)$ .** Now we derive for Eq. (4.27) based on the expansion given by Eq. (4.26). Here we use the Euler-Maclaurin formula to estimate the three sums appearing in Eq. (4.26). The first sum in Eq. (4.26) over

$0 \leq j \leq n - K - 1$  can be approximated by

$$(B.1) \quad \begin{aligned} \sum_{j=0}^{n-K-1} \frac{\zeta_j}{(\hat{x}_n - \hat{x}_j)^2} &= \sum_{j=0}^{n-K-1} \frac{\zeta(\phi^{-1}(j/N))}{(\hat{x}_n - \phi^{-1}(j/N))^2} \\ &\sim N \int_0^{\frac{n-K-1}{N}} \frac{\zeta(\phi^{-1}(\xi)) d\xi}{(\hat{x}_n - \phi^{-1}(\xi))^2} + \frac{1}{2} \left( \frac{\zeta_{n-K+1}}{(\hat{x}_n - \hat{x}_{n-K-1})^2} + \frac{\zeta_0}{(\hat{x}_n - \hat{x}_0)^2} \right) + \mathcal{O}\left(\frac{N^2}{K^3}\right), \end{aligned}$$

where the definition of  $\phi^{-1}(\xi) = \hat{x}$  if  $\phi(\hat{t}, \hat{x}) = \xi$ .

The integral appearing in Eq. (B.1) can be evaluated by using integration by part

$$(B.2) \quad \begin{aligned} \int_0^{(n-K-1)/N} \frac{\zeta(\phi^{-1}(\xi)) d\xi}{(\hat{x}_n - \phi^{-1}(\xi))^2} &= \int_{\hat{x}_0}^{x_{n-K-1}} \frac{\phi'(a)\zeta(a) dt}{(\hat{x}_n - t)^2} \\ &= \frac{\phi'(a)\zeta(a)}{\hat{x}_n - a} \Big|_{a=\hat{x}_0}^{a=x_{n-K-1}} - \int_{\hat{x}_0}^{x_{n-K-1}} \frac{(\phi'(a)\zeta(a))' da}{\hat{x}_n - a}, \end{aligned}$$

where  $\phi'(a)$  is the short form of  $\phi'(\hat{t}, a)$ . Hence the first sum in Eq. (B.1) over  $0 \leq j < n - K$  can be calculated by

$$(B.3) \quad \begin{aligned} -\frac{1}{N^2} \cdot \sum_{j=0}^{n-K-1} \frac{\zeta_j}{(\hat{x}_n - \hat{x}_j)^2} &= \frac{1}{N} \cdot \left( -\frac{\phi'_{n-K-1} \zeta_{n-K-1}}{\hat{x}_n - \hat{x}_{n-K-1}} + \frac{\phi'_0 \zeta_0}{\hat{x}_n - \hat{x}_0} \right) \\ &+ \frac{1}{N} \int_{\hat{x}_0}^{\hat{x}_{n-K-1}} \frac{(\phi'(a)\zeta(a))' da}{\hat{x}_n - a} - \frac{1}{2N^2} \cdot \frac{\zeta_{n-K+1}}{(\hat{x}_n - \hat{x}_{n-K-1})^2} + o\left(\frac{1}{N}\right). \end{aligned}$$

In analogy the first sum in Eq. (4.26) over  $n + K + 1 \leq j \leq N$  is calculated by

$$(B.4) \quad \begin{aligned} -\frac{1}{N^2} \cdot \sum_{j=n+K+1}^N \frac{\zeta_j}{(\hat{x}_n - \hat{x}_j)^2} &= \frac{1}{N} \left( \frac{\phi'_{n+K+1} \zeta_{n+K+1}}{\hat{x}_n - \hat{x}_{n+K+1}} - \frac{\phi'_N \zeta_N}{\hat{x}_n - \hat{x}_N} \right) \\ &+ \frac{1}{N} \int_{\hat{x}_{n+K+1}}^{\hat{x}_N} \frac{(\phi'(a)\zeta(a))' da}{\hat{x}_n - a} - \frac{1}{2N} \cdot \frac{\zeta_{n+K+1}}{(\hat{x}_n - \hat{x}_{n+K+1})^2} + o\left(\frac{1}{N}\right). \end{aligned}$$

Combining Eq. (B.3) and (B.4), we get the asymptotic expansion to the first sum in Eq. (4.26)

$$(B.5) \quad \begin{aligned} -\frac{1}{N^2} \cdot \sum_{\substack{0 \leq j < n-K \\ n+K < j \leq N}} \frac{\zeta_j}{(\hat{x}_n - \hat{x}_j)^2} &\sim \frac{1}{N} \cdot \left( \frac{\phi'_{n+K+1} \zeta_{n+K+1}}{\hat{x}_n - \hat{x}_{n+K+1}} - \frac{\phi'_N \zeta_{n-K-1}}{\hat{x}_n - \hat{x}_{n-K-1}} \right) \\ &+ \frac{1}{N} \cdot \left( \frac{\zeta_0}{\hat{x}_0 - \hat{x}_0} - \frac{\zeta_N}{\hat{x}_n - \hat{x}_N} \right) + \frac{1}{N} \int_{\hat{x}_0}^{\hat{x}_N} \frac{(\phi'(a)\zeta(a))' da}{\hat{x}_n - a} \\ &- \frac{1}{2N^2} \cdot \left( \frac{\zeta_{n+K+1}}{(\hat{x}_n - \hat{x}_{n+K+1})^2} - \frac{\zeta_{n-K-1}}{(\hat{x}_n - \hat{x}_{n-K-1})^2} \right) + o\left(\frac{1}{N}\right), \end{aligned}$$

where the integral is evaluated in the sense of principle value.

Similarly, if we define

$$(B.6) \quad g(a) = \phi'(a)(\zeta(a)\zeta_n - 3S^2),$$

we can asymptotically calculate the second sum in Eq. (4.26) by (B.7)

$$\begin{aligned}
& \frac{1}{N^3} \sum_{\substack{0 \leq j \leq n-K-1 \\ n+K+1 \leq j \leq N}} \frac{\zeta_j \zeta_n - 3S^2}{(\hat{x}_n - \hat{x}_j)^3} \\
& \sim \frac{1}{2N} \frac{g(a)}{(\hat{x}_n - a)^2} \Big|_{a=\hat{x}_0}^{a=\hat{x}_{n+K+1}} - \frac{1}{N} \frac{g'(a)}{\hat{x}_n - a} \Big|_{a=\hat{x}_0}^{a=\hat{x}_{n+K+1}} \\
& \quad + \frac{1}{2N} \frac{g(a)}{(\hat{x}_n - a)^2} \Big|_{a=\hat{x}_{n-K-1}}^{a=\hat{x}_N} - \frac{1}{N} \frac{g'(a)}{\hat{x}_n - a} \Big|_{a=\hat{x}_{n-K-1}}^{a=\hat{x}_N} + o\left(\frac{1}{N}\right) \\
& \sim \frac{1}{2N} \left( \frac{\phi_{n+K+1}(\zeta_{n+K+1}\zeta_n - 3S^2)}{(\hat{x}_n - \hat{x}_{n+K+1})^2} - \frac{\phi_{n-K-1}(\zeta_{n-K-1}\zeta_n - 3S^2)}{(\hat{x}_n - \hat{x}_{n-K-1})^2} \right) + o\left(\frac{1}{N}\right).
\end{aligned}$$

In a similar manner, the third sum in Eq. (4.26) is found at  $o(1/N)$ .

Therefore, incorporating Eqs. (B.5) and (B.7) into (4.26), we obtain

$$\begin{aligned}
\hat{\tau}_{\text{int}}^{\text{out}}(\hat{p}_n, 0) & \sim \frac{\phi'_{n+K+1}\zeta_{n+K+1}}{\hat{x}_n - \hat{x}_{n+K+1}} - \frac{\phi'_{n-K-1}\zeta_{n-K-1}}{\hat{x}_n - \hat{x}_{n-K-1}} + \frac{\phi'_0\zeta_0}{\hat{x}_n - \hat{x}_0} - \frac{\phi'_N\zeta_N}{\hat{x}_n - \hat{x}_N} \\
& \quad + \int_{\hat{x}_0}^{\hat{x}_N} \frac{(\phi'(a)\zeta(a))' da}{\hat{x}_n - a} - \frac{1}{2N} \cdot \left( \frac{\phi'_{n-K-1}\zeta_{n-K-1}}{(\hat{x}_n - \hat{x}_{n-K-1})^2} + \frac{\phi'_{n+K+1}\zeta_{n+K+1}}{(\hat{x}_n - \hat{x}_{n+K+1})^2} \right) \\
& \quad + \frac{1}{2N} \left( \frac{\phi_{n+K+1}(\zeta_{n+K+1}\zeta_n - 3S^2)}{(\hat{x}_n - \hat{x}_{n+K+1})^2} - \frac{\phi_{n-K-1}(\zeta_{n-K-1}\zeta_n - 3S^2)}{(\hat{x}_n - \hat{x}_{n-K-1})^2} \right) + o\left(\frac{1}{N}\right).
\end{aligned}$$

To further simplify the expansion of  $\hat{\tau}_{\text{int}}^{\text{out}}(\hat{p}_n, 0)$ , we employ

$$(B.9) \quad \hat{x}_{n-K-1} \sim \hat{x}_n - \frac{K+1}{N} \cdot \frac{1}{\phi'_n} - \frac{(K+1)^2}{N^2} \cdot \frac{\phi''_n}{2(\phi'_n)^3} + \mathcal{O}\left(\frac{K^3}{N^3}\right),$$

$$(B.10) \quad \hat{x}_{n+K+1} \sim \hat{x}_n + \frac{K+1}{N} \cdot \frac{1}{\phi'_n} - \frac{(K+1)^2}{N^2} \cdot \frac{\phi''_n}{2(\phi'_n)^3} + \mathcal{O}\left(\frac{K^2}{N^2}\right),$$

$$(B.11) \quad \zeta_{n-K-1} \sim \zeta_n - \frac{K+1}{N} \cdot \frac{\zeta'_n}{\phi'_n} + \mathcal{O}\left(\frac{K^2}{N^2}\right),$$

and

$$(B.12) \quad \zeta_{n+K+1} \sim \zeta_n + \frac{K+1}{N} \cdot \frac{\zeta'_n}{\phi'_n} + \mathcal{O}\left(\frac{K^2}{N^2}\right),$$

due to the fact that  $(K+1)/N \ll 1$ . Incorporating Eqs. from (B.9) to (B.12) into (B.8) gives rise to Eq. (4.27).

#### REFERENCES

- [1] M. ABRAMOWITZ AND I. A. STEGUN, eds., *Handbook of Mathematical Functions*, Dover Publications, Inc., New York, 10th ed., 1972.
- [2] A. ACHARYA, *A model of crystal plasticity based on the theory of continuously distributed dislocations*, J. Mech. Phys. Solids, 49 (2001), pp. 761–784.

- [3] S. BRINCKMANN AND E. VAN DER GIESSEN, *A discrete dislocation dynamics study aiming at understanding fatigue crack initiation*, Mater. Sci. Eng. A - Struct., 387 (2004), pp. 461–464.
- [4] B. CHENG, H. S. LEUNG, AND A. H. W. NGAN, *Strength of metals under vibrations - dislocation-density-function dynamics simulations*, Philos. Mag., (2014), pp. 1–21.
- [5] D. DICKEL, K. SCHULZ, S. SCHMITT, AND P. GUMBSCH, *Dipole formation and yielding in a two-dimensional continuum dislocation model*, Phys. Rev. B, 90 (2014), p. 094118.
- [6] A. EL-AZAB, *Statistical mechanics treatment of the evolution of dislocation distributions in single crystals*, Phys. Rev. B, 61 (2000), pp. 11956–11966.
- [7] M. G. D. GEERS, R. H. J. PEERLINGS, M. A. PELETIER, AND L. SCARDIA, *Asymptotic behaviour of a pile-up of infinite walls of edge dislocations*, Arch. Ration. Mech. Anal., 209 (2013), pp. 495–539.
- [8] I. GROMA, *Link between the microscopic and mesoscopic length-scale description of the collective behavior of dislocations*, Phys. Rev. B, 56 (1997), pp. 5807–5813.
- [9] I. GROMA, F. F. CSIKOR, AND M. ZAISER, *Spatial correlations and higher-order gradient terms in a continuum description of dislocation dynamics*, Acta Mater., 51 (2003), pp. 1271–1281.
- [10] C. L. HALL, S. J. CHAPMAN, AND J. R. OCKENDON, *Asymptotic analysis of a system of algebraic equations arising in dislocation theory*, SIAM J. Appl. Math., 70 (2010), pp. 2729–2749.
- [11] A. K. HEAD, S. D. HOWISON, J. R. OCKENDON, AND S. P. TIGHE, *An equilibrium-theory of dislocation continua*, SIAM Rev., 35 (1993), pp. 580–609.
- [12] J. P. HIRTH AND J. LOTHE, *Theory of dislocations*, Wiley, New York, 2nd ed., 1982.
- [13] T. HOCHRAINER, S. SANFELD, M. ZAISER, AND P. GUMBSCH, *Continuum dislocation dynamics: Towards a physical theory of crystal plasticity*, J. Mech. Phys. Solids, 63 (2014), pp. 167–178.
- [14] H. MUGHRABI, *Microscopic mechanisms of metal fatigue*, in Proc. 5th Int. Conf. on the Strength of Metals and Alloys, vol. 3, Pergamon, Oxford, 1980, p. 1615.
- [15] H. OCKENDON AND J. R. OCKENDON, *Dynamic dislocation pile-ups*, Philos. Mag. A, 47 (1983), pp. 707–719.
- [16] R. E. VOSKOBOINIKOV, S. J. CHAPMAN, J. R. OCKENDON, AND D. J. ALLWRIGHT, *Continuum and discrete models of dislocation pile-ups. i. pile-up at a lock*, J. Mech. Phys. Solids, 55 (2007), pp. 2007–2025.
- [17] Y. XIANG, *Continuum approximation of the peach-koehler force on dislocations in a slip plane*, J. Mech. Phys. Solids, 57 (2009), pp. 728–743.
- [18] X. H. ZHU AND Y. XIANG, *Continuum model for dislocation dynamics in a slip plane*, Philo. Mag., 90 (2010), pp. 4409–4428.
- [19] ———, *Continuum framework for dislocation structure, energy and dynamics of dislocation arrays and low angle grain boundaries*, J. Mech. Phys. Solids, 69 (2014), pp. 175–194.
- [20] Y. C. ZHU AND S. J. CHAPMAN, *A natural transition between equilibrium patterns of dislocation dipoles*, J. Elast., 117 (2014), pp. 51–61.
- [21] Y. C. ZHU, H. Q. WANG, X. H. ZHU, AND Y. XIANG, *A continuum model for dislocation dynamics incorporating frank-read sources and hall-petch relation in two dimensions*, Int. J. Plast., 60 (2014), pp. 19–39.
- [22] Y. C. ZHU AND Y. XIANG, *A continuum model for dislocation dynamics in three dimensions using the dislocation density potential functions and its application in understanding the micro-pillar size effect*, Submitted for publication.